UNIVERSITY OF OKLAHOMA

GRADUATE COLLEGE

DEVELOPMENT OF NON-PROPRIETARY ULTRA-HIGH-PERFORMANCE CONCRETE MIX DESIGNS

A THESIS

SUBMITTED TO THE GRADUATE FACULTY

in partial fulfillment of the requirements for the

Degree of

MASTER OF SCIENCE

By

AMY S. MCDANIEL
Norman, Oklahoma
2017

DEVELOPMENT OF NON-PROPRIETARY ULTRA-HIGH-PERFORMANCE CONCRETE MIX DESIGNS

A THESIS APPROVED FOR THE
SCHOOL OF CIVIL ENGINEERING AND ENVIRONMENTAL SCIENCE

BY

_____
Dr. Jeffery S. Volz, Chair

_____
Dr. Royce Floyd

_____
Dr. Gerald Miller

Acknowledgements

I would like to acknowledge the members of the research team that put in the time and effort to make this thesis a success, including Trevor Looney, C.J. Alsenay, and Mitchel Gordon. I would also like to acknowledge Dr. Volz, who guided me through this project, and Mike Schmidt, who makes using Fears Lab manageable. Finally, I would like the acknowledge my husband Charlie, who spent many hours of his weekend at the lab helping me complete this project.

Table of Contents

List of Tables

List of Figures

Abstract

Ultra-High-Performance Concrete (UHPC) is defined by the Federal Highway Administration (FHWA) as having a compressive strength of 21.7 ksi (kilo-pounds per square inch), a post-cracking tensile strength 0.72 ksi, and high flowability. This product is desired by the Oklahoma Department of Transportation (ODOT) to construct durable deck joints, both for repair and use on new bridges. However, commercial UHPC is prohibitively expensive. This study sought to develop a cost-effective, non-proprietary mix design for UHPC using materials accessible in the State of Oklahoma.

Mix designs were iterated from the baseline of non-proprietary mix designs formulated for other regions of the U.S. The concept of particle packing, which seeks to optimize the combination of constituent gradations in order to minimize empty air space, was also employed to develop a mix with the properties of UHPC. Nine iterative groups, Series A through Series J, sought to produce the optimal combination of SCMs, the aggregate/cementitious material ratio, the water/cementitious material ratio, and the dosage of high-range water reducer. The three mixes strongest in compression were selected to add fiber reinforcement and study the effect of heat curing. Properties key to its use on bridge joints, including bending and elasticity, were tested.

While this study did not produce a mix design meeting the FHWA definition of UHPC, a cost-effective non-proprietary mix design was established that has high mortar flow, a first-cracking tensile strength of 2.0 ksi, and a compressive strength exceeding 20 ksi at 3 days with heat curing. Additionally, field replicable mixing, placing, and curing procedures were developed for use in repairing bridge joints and future applications.

1 Introduction

This chapter will introduce the reasons for developing a non-proprietary ultra-high-performance concrete (UHPC) using materials available in the State of Oklahoma. Additionally, this section includes a discussion of the scope, objectives, and goals of this research study, as well as providing an outline of this thesis.

1.1 Background and Justification

Ultra-high-performance concrete (UHPC) was first introduced approximately 25 years ago when the Lafarge product Ductal® came onto the market. Ductal® has since dominated the market, and much of the research in the use and application of UHPC uses the product as their baseline. However, this product is expensive, with a price tag reaching $3,200 per cubic yard, including the services that come with the product. To compare, a typical concrete mix costs about $150 per cubic yard, making Ductal® nearly 20 times more expensive than typical concrete. The significant cost of commercial UHPC has inspired researchers around the country, including the Army Corps of Engineers and the Federal Highway Administration (FHWA), to develop more cost-effective mix designs with materials available at several locales strategic to these organizations. The FHWA internally defines UHPC as having a compressive strength of 21.7 kilo-pounds per square inch (ksi), and a sustained post-cracking tensile strength of at least 0.72 ksi after the addition of steel fibers (Graybeal, 2011). This definition is widely accepted in the concrete industry.

The UHPC developed is this study is intended specifically for use in replacing joints in existing concrete bridges. However, UHPC is being used in an increasing variety of applications, including precast panel joints, pi-shaped beams, ultra-thin

pedestrian bridge decks, ultra-thin waffle slabs, noise barrier panels, seismic retrofit of bridge columns, and precast tunnel segments (Graybeal, 2014). Most of these developments are being explored in Europe, where its use is more common, due to huge investments in the technology by Germany (Russel and Graybeal, 2013). In the United States, the primary use is connecting precast elements in bridges, and the material has been used by at least seven state Departments of Transportation (DOT) and extensively by the New York DOT (Graybeal, 2014).

UHPC is composed of cement, supplementary cementitious materials (SCMs), fine aggregates, and high range water reducers (HRWR). These constituents must be combined to produce a mix design that has adequate mortar flow, strength, and economy. SCMs can include fly ash, silica fume, ground-granulated blast furnace slag (GGBFS), and VCAS™. SCMs are critical, given they increase the long-term strength of the concrete, improve the durability of the concrete, and typically improve the economy of the mix. While not a primary design consideration, SCMs are recycled, and have a significantly reduced carbon impact compared to carbon cement (Radlinkski et al., 2011). Fine aggregates are typically a combination of natural and manufactured sands. HRWRs are typically polycarboxylate-based, and are used to reduce water demand and increase workability. Reduced water/cementitious material (w/cm) ratios of UHPC demand high shear mixing methods, usually for extended mixing times.

Steel fiber reinforcement is used in almost all field applications. A consistent curing regimen is also necessary to produce the desired properties. The saturation of the concrete surface, the pressure, and the temperature can all have significant impact on

the final cured properties of the UHPC and must be carefully controlled, especially in variable field conditions (Graybeal and Tanesi., 2007; Yang et al., 2009).

Because small changes can have a large impact on the final properties of UHPC, every aspect of the mix design, reinforcement, mixing method, and curing regimen must be carefully controlled to obtain the desired results. However, the uses of UHPC can easily justify the additional costs and inconvenience. The high mortar flow makes it easier to place in hard-to-reach, small places, though the formwork must be watertight. In bridge joint repair and connections of precast deck panels, significantly less rebar lap length is necessary, as the UHPC leads to a much shorter tensile development length than typical concrete (Graybeal, 2014). The high early strength may enable bridges to open earlier after repairs and get cars back on the road sooner. While this product will be used judiciously, the advantages of flowability, simpler lap-splice connections, and significant increases in durability will make UHPC a useful addition of the arsenal of problem-solving tools available to ODOT.

1.2 Project Scope

This research focuses on the development of a non-proprietary UHPC mix design using materials available in the State of Oklahoma, as well as defining a mixing, placing, and curing procedure that would maximize the performance of the UHPC and be field replicable. Additionally, this research seeks to define the properties that would be pertinent to its use as joint repair material in Oklahoman bridges.

1.3 Objectives and Goals

1.3.1 Objectives

1. Develop concrete mix designs that meet the FHWA definition of UHPC using locally available materials in the State of Oklahoma (Graybeal, 2011).
2. Optimize concrete mix designs that would reduce the cost of materials and concrete placement.
3. Develop a mixing, placing, and curing method that optimizes UHPC performance and is repeatable in the field.

1.3.2 Goals

The goal of this research is to develop a UHPC mix design and implementation procedure, using affordable, locally available materials.

1.4 Outline

This thesis consists of six chapters. Chapter 1 provides a brief background and justification for the study, as well as an outline of the scope, objectives, and goals of the research. Chapter 2 summarizes the literature relevant to study, including the topics of particle packing, material properties and chemical combinations, optimal water/cementitious materials ratio, fiber reinforcement, mixing procedure, and curing regimen.

Chapter 3 outlines the development of mix designs through an iterative process. Chapter 4 investigates the effect of heat curing and fiber reinforcement on the performance of UHPC. Chapter 5 establishes the non-compressive properties of the UHPC that would be pertinent to its use on highway bridges, including modulus of

elasticity (MOE), modulus of rupture (MOR), and abrasion resistance. Chapter 6 summarizes the findings, conclusions, and recommendations of the research study.

2 Literature Review

2.1 Introduction

This chapter contains a review of the literature related to the development and testing of UHPC. There are many factors influencing the ultimate strength of the concrete related to the mix design, including the particle packing of the constituents, chemical interactions, cementitious activation, water/cementitious materials (w/cm) ratio, and amount and type of fibers. Small differences in gradation from material sources can have a large impact on the properties of the fresh and hardened concrete, making it difficult to directly repeat findings of other authors. There are also several procedural factors that are reported to affect the fresh and hardened properties of the concrete, such as mixing procedure and curing regimen. These subjects were reviewed in the following chapter.

2.2 Particle Packing

Mix design is the most critical factor in achieving UHPC strength and durability. One of the primary mechanisms by which UHPC reaches its high strength is through dense particle packing. Dense particle packing is achieved by packing gradually smaller particles into the voids between the natural packing of large particles, limiting the space in which air voids can exist (Aghdasi et al., 2016). Air space is the weakest constituent in any composite mixture. There are several physical particle-combination optimizing strategies, including discrete element models, particle packing models, and optimization curves (Fennis and Walraven, 2012). As optimization curves were the most frequently

cited approach based on a review of the applicable literature, and since they are more accessible than the other methods, they were chosen for this current study on UHPC.

Theoretically, optimization curves work to create the highest packing density by combining optimal amounts of differently sized particles (Fennis and Walraven, 2012) Though some version of optimization curves for concretes have been around since 1892, the Andreasen and Andersen curve is the modern foundation for this particle optimization strategy (Brouwer and Radix, 2005). The Andreasen and Andersen model takes the optimum packing to be when the cumulative particle size distribution follows the function for packing established by Equation 2.1,

$$P(D) = \left(\frac{D}{D_{max}}\right)^q \qquad \text{Eq. 2.1}$$

where P is the fraction of the mix solids that should be smaller than size D, D_{max} is the maximum particle size in the mix, and q is the distribution modulus (Andreasen and Andersen, 1930). This curve was developed to optimize typically sized concrete aggregates, which have large, angular particles. The optimal q value was determined experimentally to fall within the range of 0.33 – 0.50, with more angular particles generally requiring a lower distribution modulus (Fennis and Walraven, 2012; Brouwers and Radix, 2005).

Because the Andreasen and Andersen curve does not consider the lower particle size limit, a modified curve (Equation 2.2) was proposed by Funk and Dinger to accommodate the minimum particle size:

$$P(D) = \frac{D^q - D_{min}^q}{D_{max}^q - D_{min}^q} \qquad \text{Eq. 2.2}$$

where D_{min} is the minimum particle size of the constituents in the mix (1994). While the Andreasen and Andersen curve is still used, the modified model proposed by Funk and Dinger is the standard used for both self-consolidating concrete and UHPC. While this is the consensus model, there is no consensus of the most optimal distribution modulus. *Q*-values of 0.25 to 0.30 yield the highest strength mixes, and *q*-values less than 0.23 yield the most workable mixtures (Sbia et al., 2016; Yu et al., 2015). For UHPC mix design, target *q*-values of 0.25, 0.23, and 0.22 have been used (Sbia et al., 2016; Yu et al., 2015; Kim et al., 2016, respectively).

There are several weaknesses of this method, the first and most obvious being that the particles considered in this model are dry. Additionally, this model does not consider any gel pores, chemical admixtures, or chemical interaction of any kind. The particle packing models and discrete element models also share these same weaknesses.

There are several analytical ways to model the particle packing and gradation optimization of the concrete constituents. A common particle packing software is EMMA, which uses the modified Andreasen model to display a cumulative particle size distribution. EMMA's popularity is caused, in part, because it is free, but the software only produces graphical output. Effective analysis with the program is only possible when used in conjunction with a data analysis software that can create computational output from the graphic output (Yu et al., 2015).

The 4C packing software also uses the linear packing density model to determine particle packing density based on particle size distribution (Sbia et al., 2016). This software may be more useful given that it provides both graphic and numeric output. Sbia noted that the mixes improved when refined with the software, but the ideal curves

anticipated by the program were not helpful in isolation, given the program could not anticipate the chemical interplay and hydration (2016). Additionally, Sbia noted that mixes with near-optimal particle packing had some capacity of flow without the use of high-range water reducer (HRWR) (2016).

Using a modified Andreasen and Andersen curve to optimize the gradation of particles so that that they pack densely is a well-established method to formulate a UHPC paste. To effectively optimize mixes, a computer program is necessary. This method, like all particle optimization methods, does not consider chemical interplay.

2.3 Material Properties and Chemical Combinations

Replicating a published UHPC mix design is difficult, given that authors encounter aggregates and cementitious materials that have different particle sizes and shapes, varying chemical compositions, and different superplasticizers. Authors have noted the lack of repeatability of published mixes (Sbia, et al., 2016; Ghafari et al., 2015). There are four categories of materials in UHPC: water, HRWRs, cementitious materials, and fillers, which in typical concrete would be referred to as aggregate. In practice, most UHPC mixes have w/cm ratios so low that some of the cementitious material will not be hydrated, and will be used as inert filler. However, given there is little to no control of which and how much of each cementitious material will hydrate, these materials are considered separately.

Inert fillers are critical to the formulation of UHPC. Given that a significant portion of the cementitious material in UHPC with remain inert, it is more beneficial to the overall mix to have strong, high performance powders than unhydrated cements.

However, the chemical composition and performance of these powders can vary considerably.

Sand is the most common constituent, given it is the cheapest material in UHPC. Quartz sand, made of primarily silica, plus impurities, is hard and strong. There are many different types of sand available, in many levels of cleanliness and gradations. Studies have been conducted with the purposes of finding a mix design that can achieve the properties of a UHPC with a local sand source, and each attempt showed that it was possible (Alsalman et al., 2017; Graybeal and Tanesi, 2007; Yang et al., 2009; Yu et al., 2015).

There are also many manufactured silica-based products that have a very tightly controlled gradation, going by names such as silica powder, quartz flour, glass powder, ground quartz, and quartz powder (Alsalman et al., 2017; Aghdasi et al., 2016; Fennis and Walraven, 2012; Kim et al., 2016). These products have advantages over ordinary sand including increased purity and a more controlled gradation. However, when manufactured silica products replace ordinary sand, the cheapest constituent, it is being replaced with a constituent that is considerably more expensive.

There have been experiments with filler materials other than manufactured silica products. Ground limestone powder has been used as an inert filler, and it is possible it possesses some cementitious properties (Yu et al., 2015). Electric arc furnace oxidizing slag has been found to increase flowability, though it reduces strength over natural sand (Kim et al., 2016). Recycled glass cullet has been used, though its mechanical properties were inferior to that of ordinary sand (Yang et al., 2009).

Supplementary cementitious materials are also essential in the formulation of UHPC. Silica fume, which in present in every UHPC mix, is recommended in different proportions. As little as 10% silica fume has been found to produce mixes that meet the criteria for UHPC (Ye et al., 2012; Ibrahim et al., 2013). Levels of silica fume exceeding 10% have been reported to increase water demand, reduce workability, and produce "sticky" mixes (Ghafari et al., 2015; Ibrahim et al., 2013). Graybeal, in a study that developed seven (7) non-proprietary UHPC mixes using materials from different regions in the U.S., recommended 17% replacement of silica fume for all regions (2013). Most authors reported best results with replacements higher than 20%, and even up to 30% (Alkaysi and El-Tawil, 2015; Alsalman et al., 2017; Sbia et al., 2016).

Fly ash and ground granulated blast furnace slag (GGBFS) were the most common proprietary supplementary cementitious materials. Mixes with silica fume, fly ash, and GGBFS did not perform as well as mixes with either silica fume and fly ash or silica fume and GGBFS (Aghdasi et al., 2016). Fly ash has been cited to reduce the heat of hydration, as well as increase mortar flow (Aghdasi et al., 2016). Replacing cement with fly ash has been reported to increase the compressive strength at 28 days by up to 20%, though there are more conservative reports that cite only a 10% increase over the control strength at 90 days (Aghdasi et al., 2016; Ibrahim et al., 2017). However, GGBFS replacements were found to produce stronger mixes than comparable levels of fly ash at high and low replacement levels (Ibrahim et al., 2013, Sbia et al. 2016). GGBFS is noted to reduce water demand and produce superior mechanical properties at 28 days and 91 days compared to the control and comparable replacements of fly ash (Yu et al., 2015).

2.4 Water-Cementitious Material Ratio

2.4.1 Fresh Concrete Properties

The w/cm ratio is one of the most important parameters in UHPC mix design. The amount of water determines how much of the cementitious material is hydrated, and how much acts as an inert filler. The ACI field reference manual states that the theoretical w/cm ratio required to fully hydrate the cement is 0.21 to 0.28, though this does not consider the amount of water required to hydrate the supplementary cementitious materials in their secondary reactions or the amount required to fill gel pores (ACI, 2015).

The optimal w/cm in mixes with silica fume as the only SCM is reported to be in the range of 0.18 to 0.208 (Aghdasi et al., 2016, Yu et al., 2015). The optimal w/cm ratios for low levels of fly ash is reported to be 0.176 to 0.200, and the optimal w/cm ratio for mixes with low GGBFS replacements is reported to be 0.18 (Aghdasi et al., 2016, Yu et al., 2015). However, it is difficult to compare w/cm ratios directly, given that widely different amounts of HRWR are used in the mixes, and the water demands vary significantly between each SCM.

The amount of superplasticizer used is critical to the w/cm ratio, given that high strength and a high mortar flow are two key properties of UHPC. There are both polycarboxylate-based HRWRs and phosphonate-cased HRWRs that are stated to perform at the levels desired to develop UHPC, but only polycarboxylate HRWR were cited in this literature study (Graybeal, 2013). Dosages of HRWR vary from 1.92 lb/yd^3 (30.7 kg/m^3) to 3 lb/yd^3 (48 kg/m^3), but different brands of HRWR vary such that a

direct comparison is not useful (Alsalman, et al., 2017; Alkaysi and El-Tawil, 2015; Ye et al., 2012; Graybeal, 2013).

2.5 Fiber-Reinforcement

Most of the previously-mentioned research has studied how to maximize the compressive strength of the UHPC. However, one of the primary benefits of UHPC is high post-cracking tensile strength. This high post-cracking tensile strength is achieved through steel fiber reinforcement, which is typical in UHPC. While this is technically ultra-high-performance fiber reinforced concrete (UHPFRC), steel fibers are so common that the extra designation is often dropped.

Steel fibers can increase the ultimate tensile strength (considering failure to be the load at which the specimen breaks into two pieces) by up to 75% (Ye et al., 2012). Steel fibers in UHPC can be typical steel fibers, which are thick, uncoated, and either crimped, twisted, or hook-ended, or, they can be coated, straight, wire-drawn fibers. The geometry of the steel fibers can have a significant impact of the ultimate tensile strength gain. End-hooked long fibers have the most effective gain compared to short and long wire-drawn fibers, as well as typical short fibers (Ye et al., 2012). Micro straight fibers provide slightly superior peak post-cracking tensile strength compared to short twisted fibers (Aghdasi et al., 2016).

While fibers increase the ultimate tensile strength considerably, there is almost no benefit in the first cracking strength (Aghdasi et al., 2016; Graybeal, 2006). Though compressive strengths are not the primary beneficiaries of steel fibers, fiber reinforcement can increase compressive strength (Alsalman et al, 2017).

Ductility and tensile benefits have been found in increasing fiber proportions up to 4%, though workability concerns often make the fiber proportion of 2% by volume the optimal fiber reinforcement (Alsalman et al., 2017; Graybeal and Tanesi, 2007; Yang et al., 2015; Ye et al., 2012). While 2% has been found to be the most effective fiber reinforcement ratio, a proportion of 1.5% was recommended as the optimal balance between ductility and cost effectiveness (Graybeal, 2013).

Most UHPC developed for field use is fiber reinforced. Wire drawn fibers and more typical steel fibers are both used to increase the ultimate tensile strength of a member. There is small enhancement in compressive strength due to the fibers, but they are primarily used for tensile benefit.

2.6 Mixing Procedure

The low w/cm ratio of UHPC requires a high-shear mixer and specialized mixing procedures. There is no procedural standard for mixing, given that the mixers used in different labs deliver different speeds of shear. Low shear mixers can deliver similar results to high shear mixers, but the mixing time must be significantly increased (Graybeal, 2006). Typically, mixing takes 15 to 20 minutes total. The dry constituents are always blended, fine aggregates oven-dry, for 5 to 10 minutes before gradually adding the water and high-range water reducer. Most researchers added fibers several minutes after the paste had come together (Kim et al., 2016; Allena and Newston, 2012, Alsalman et al., 2017; Yang et al., 2009). The temperature of the constituents may be as influential as the mixing method. Adding chilled water vs. room temperature water has been found to increase mixture workability, and cubed ice is said to “increase the

efficiency of the mixing process by providing a sustained supply of water throughout the mixing process… as the ice melts" (Graybeal, 2014).

Consolidation methods also vary, though consolidation can have a significant impact on the compressive strength. In general, authors that studied the cement paste matrix vibrated specimens on high frequency vibration tables, and those that included fibers did not consolidate (Allena and Newston, 2012; Graybeal, 2006; Kim et al., 2016; Yang et al., 2009). There is concern that vibrating the concrete excessively may cause segregation of the fibers, aligning them and making them far less effective (Graybeal, 2006; Yang et al., 2009).

The mixing procedure for UHPC is more involved that typical concrete. Greater shear is required to mix the constituents, and mixes take more time to fully develop the preferred rheological properties. Mixes without fibers are typically consolidated. Mixes that include fibers typically are not consolidated, given over consolidated mixes align fibers and make them less effective.

2.7 Curing Regimes

The effect of different curing regimens has been studied. Pressurized steam curing is the best curing method, yielding increased compressive strengths, tensile cracking strengths, and elastic moduli compared to dry curing, heat curing, and moist curing (Graybeal, 2006). Additionally, steam-cured and heat-cured specimens both showed an increase in abrasion resistance and durability over moist-cured specimens (Graybeal and Tanesi, 2007). Steam curing and heat curing for only a short amount of time, applied as many as 15 days after casting, has shown to produce some benefit (Graybeal, 2006).

While steam curing is the most beneficial, there are significant benefits of heat curing. Common temperatures of heat curing are 194°F (90°C), 140°F (60°C), and the typical baseline temperature of 68°F (20°C) with >95% humidity. (Alsalman et al., 2017; Graybeal and Tanesi, 2007; Sbia et al., 2016). Heat curing at 90°C for 7 days has been shown to lead to a 10% improvement of tensile strength at 28-days, in addition to improved fracture energy over the specimens cured at 20°C (Yang et al., 2009). Heat curing significantly increases the rate at which the concrete cures. Specimens cured at 90°C for 7 days saw nearly no improvement from 7 days to 91 days in either compressive or tensile strength. The specimens cured at 20°C for 7 days gained strength at a normal pace, but even at 91 days did not reach the performance of the 90°C specimens (Yang et al., 2009).

Heat and steam curing both significantly accelerate the curing of the concrete, producing superior durability and strength properties in a truncated time frame. Any amount of heat or steam applied within the first two weeks of curing has shown to provide strength and durability benefits. The literature in the study did not indicate any long-term detriments.

3 Mix Design Development

3.1 Introduction

This section reports on the development of UHPC mix designs using locally available materials. The nature of this research was not such that direct iterations or improvements could be made in each experimental series, but the investigations of each series directed the information sought by the next series. This process involved a succession of nine iterative Series, A to J, in which a total of 158 mixes were designed and tested. In this development phase, compressive strength and mortar flow were the two primary design targets. While the mortar flow targets were achieved, there was no mix through this preliminary investigation that achieved the 22 ksi compressive strength design target.

3.2 Material Acquisition and Selection

As suggested by the literature, the compressive strength of UHPC is met by combining the materials optimally for two competing physical factors. The cements, supplementary cementitious materials (SCMs), and aggregates must achieve high particle packing density in order to effectively use the unhydrated particles to reduce air in the mortar paste. Additionally, the chemical reactions between the SCMs and cements must be compatible. Cement reacts with water to form the desirable product calcium silicate hydrate (CSH), which produces strength in the concrete, and calcium hydroxide (CH), an undesirable product that does not provide strength (“Supplementary”, 2016). SCMs can consume the CH and produce CSH, as well as

produce CSH directly. There must be a complimentary ratio of SCMs to cement in order to maximize the production of CSH and minimize the leftover CH.

The cements used in this research were Type I cement provided by Dolese and Type III cement provided by Buzzi Unicem. Cement is typically manufactured by combining crushed limestone, clay, and other materials in large, typically rotating, kilns. After the mixture is sufficiently hot, the product, clinker, is discharged and crushed into the final gradation. This process produces an angular particle for any gradation (Van Dam, 2013). Cement is completely hydraulic, meaning it produces CSH and CH in the presence of water but does not consume any CH. Type I and Type III cements are made from the same clinker and are chemically the same, though obtaining them from different production facilities may produce slightly different chemical profiles. Type III cement is crushed finer than Type I, has a higher specific surface, and reaches the 28-day strength of Type I cement in 7 days. The long-term strength of the cements is reportedly the same.

The Class C Fly Ash was provided by Dolese. Fly ash is a byproduct of coal-fired power plants. During combustion, the non-carbon minerals in the coal fuse together and are carried away by exhaust. These fused particles cool and solidify in the air, creating glassy, spherical particles that are finer than cement. Class C fly ash produces both hydraulic (CSH) reactions, like cement, and pozzolanic reactions. A pozzolanic reaction consumes water and CH, the undesirable product of hydraulic reactions, and produces additional strength-producing CSH. In addition to providing additional late strength due to the pozzolanic reaction, fly ash is generally considered to provide additional benefits including increased economy, increased sulfate resistance,

alkali-silica reaction (ASR) mitigation, decreased shrinkage, and decreased permeability ("Supplementary", 2016). The fly ash increases the mortar flow because the spherical particles flow over each other more easily than the angular particles of cement, like ball bearings. Like most pozzolans, fly ash depresses early strength gain.

Two separate batch samples of ground-granulated blast-furnace slag (GGBFS) were provided by the LafargeHolcim South Chicago Plant. The GGBFS, also known as slag cement, is a byproduct of the iron purification process. The slag is developed when "pig iron is extracted from the iron ore and the remaining molten material (slag) is directed into a granulator, in which water quenches the material to form glassy, sand-like particles of amorphous oxides" which are then ground to size similar to cement particles, though more angular (Van Dam, 2013). GGBFS is hydraulic and produces CSH. Though not technically a pozzolan, GGBFS provides the same benefits as a pozzolan by consuming CH and trapping alkalis in its hydration products ("Supplementary", 2016). GGBFS can be used at higher replacement rates than fly ash, is cheaper than cement, and provides other benefits such as increased late strength gain, reduced permeability, and ASR mitigation (Van Dam, 2013). GGBFS reacts more slowly than cement, retarding early strength gain.

The VCAS™ 140 White Pozzolans were purchased from Vitro Minerals. The production of this product is not as transparent as the other SCMs, though the process of production described on the website closely matches that of GGBFS. The benefits of VCAS™ 140 are advertised as the same as GGBFS, such as an increase in late-developed strength, improved resistance to sulfates and ASR, and reduced permeability (VCAS™ White Pozzolans). The cost of this material is significant compared to

GGBFS. The advantage of this product over other, cheaper SCMs is a consistent gradation and chemical composition.

Two separate batch samples of undensified silica fume were provided by Norchem. Silica fume is a byproduct of the silicon alloy production process. Like fly ash, exhaust fumes push away the particles from the arc furnaces, creating the spherical particle typical of an air-cooled product. Silica fume is entirely pozzolanic. Unlike fly ash, VCAS™, and GGBFS, all of which slow strength gain, silica fume accelerates the hydration of cement by creating nucleation sites for the CSH and CH to form. Silica fume has a very fine particle size that increases the packing density of the cement paste, and is the only SCM fine enough to consume CH at the interfacial transition zone (Van Dam, 2013). Silica fume provides benefits like significantly decreasing permeability and ASR and sulfate attack mitigation, but the primary benefit is increased strength. However, the increased specific surface of silica fume can increase the water demand that may require significant high-range water reducer (HRWR) dosages to overcome, and high replacements can result in a sticky, unworkable mixture. The price is considerably higher than cement and other SCMs.

U.S. Silica Company provided the ground silica, also known as quartz powder, in both sizes of 10 and 15-micron top size. These products are primarily considered in UHPC because they have a very fine, uniform and predictable gradation. This product phased out after one iteration, given its lack of advantage and significant expense compared to the other aggregate, masonry sand.

Metro Materials, a material supply company in Norman, Oklahoma, provided the masonry sand. Masonry sand was selected for its lack of fines, standardized

gradation according to ASTM C33, and broad availability. The sand was dried to ensure the dry constituents could be blended together without hydrating any of the cementitious materials.

The chemical compatibility component of developing UHPC was determined experimentally. While general chemical compositions of cement and SCMs are available, the precise chemical composition of the fly ash, GGBFS, and silica fume are known to vary slightly from batch to batch. The physical compatibility of the constituents, or the constituent's particle packing potential, could be more accurately determined in this study. A Beckman Coulter LS 13 320 single wavelength laser diffraction particle size analyzer produced the gradation for each of the constituents. The particle analyzer provided 92 data points between 2000 to 0.3752 micrometers, such that there is high gradation data for each constituent. The gradations for these constituents are shown in Figure 3.1.

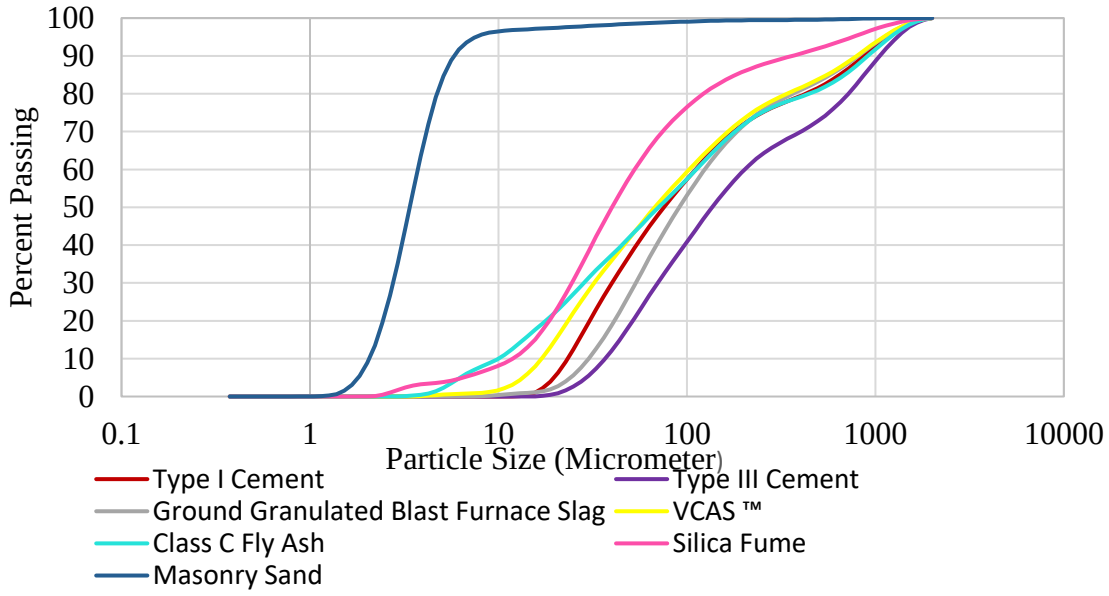

Figure 3.1 Particle Gradation of UHPC Constituents

A summary of the key properties of the constituents used in this experiment is provided in Table 3.1.

Table 3.1 Key Properties of UHPC Constituents

	Type I Cement	Type III Cement	Class C Fly Ash	Silica Fume	GGBFS	VCAS	Masonry Sand
Reaction Type	Hydraulic	Hydraulic	Hydraulic/ Pozzolanic	Pozzolanic	Acts Pozzolanic	Pozzolanic	None
Shape of Particle	Angular	Angular	Spherical	Spherical	Angular	Angular	Angualr
Specific Gravity	3.15	3.15	2.38	2.22	2.97	2.6	2.63
Early Strength	-	↑	↓	↑↑	↓	↓	n/a
Long-Term Strength	-	-	↑	↑↑	↑	↑	n/a
D10 (μm)	0.86	0.71	0.82	2.08	0.92	0.94	128.71
D50 (μm)	9.94	5.51	10.60	18.75	8.25	11.13	222.12
D90 (μm)	32.25	20.40	75.17	63.13	24.96	44.31	364.98

The last element used in the formulation of UHPC is HRWR, or superplasticizer. The HRWR used in this experiment is Glenium 7920, acquired from Dolese. This product is a polycarboxylate and can reduce water needs by ensuring the water molecules are evenly dispersed. The HRWR is critical to developing UHPC, because high mortar flows are targeted even with low water/cementitious material (w/cm) ratios.

3.3 Establishing A Mix Design Baseline

The first mixes were that of Series A, which sought to establish a baseline mix on which to iterate. Graybeal formulated cost-effective mix designs using proprietary materials for different regions in the country, though Oklahoma was in none of these regions. The mixes Q and NE most closely matched the materials available in Oklahoma and were selected to produce a baseline. One other mix was chosen based on unpublished research by Dr. Floyd. The initial trial mixes are shown in Table 3.2.

Table 3.2 Series A Baseline Mix Design Proportions

	A2	**A3**	**A4**
	Graybeal Q	**Graybeal NE**	**Floyd**
Type III Cement	0.67	0.67	0.75
Silica Fume	0.167	0.168	0.15
Fly Ash	0.163	0.162	0.1
w/cm	0.23	0.23	0.18
agg/cm	1.00	1.00	0.75
HRWR (oz./cwt)	21	22	22

These trial mixes were mixed in 0.1 ft^3 batches with a Blakeslee planetary mixer using the paddle attachment, as shown in Figure 3.2. Mortar flow measurements were taken according to ASTM 1437, as shown in Figure 3.3. The following mixing procedure was chosen based on that of similar research (Graybeal, 2006):

1. 0:00 – 0:10 minutes: blend dry constituents at low speed
2. 0:10 – 0:12: add water mixed with half HRWR, gradually, at low speed
3. 0:12 – 0:13: run at low speed
    a. Scrape bowl
4. 0:13 – 0:14: add last half of HRWR, at low speed
5. 0:14 – 0:17: run at low speed
    a. Scrape bowl
6. 0:17 – 0:19: run at medium speed
7. Establish if additional mixing time is required
8. Conduct mortar flow test
    a. Please note a 10 in. mortar flow table was used. Measures marked as 10 in. are greater or equal to 10 in.
9. Place in molds

These mixes were cast in 2 in. x 2 in. x 2 in. cube molds that were lightly greased. The twelve specimens cast for each batch were demolded at 22 ± 2 hours. The excess concrete on the sides was chipped off using a pallet knife, and the testing surface of the cubes was sanded smooth with a pumice stone. This early iteration was tested only at 1, 3, and 7 days, within the ASTM C109 recommended time frame. The iterative turnaround could be truncated because the primary cementitious material, Type III cement, gains nearly full strength at 7 days, as opposed to the typical 28 days required of Type I cement. The cubes were tested in compression at a rate of 200 to 400 lb/s after an initial preload of 50% of the expected strength, as per ASTM C109.

Figure 3.2 Mixing Dry Constituents in Blakeslee Planetary Mixer with Paddle Attachment

Figure 3.3 Conducting a Mortar Flow Test

The compressive strength data for these three initial trial mixes is shown in Figure 3.4. Neither of the mixes developed by the FHWA (A2, A3) achieved half the strength reported by Graybeal, and the Floyd mix (A4) also underperformed. This result is likely due to the slight differences in particle size and chemical composition of cements and SCMs, as well as difference in HRWR.

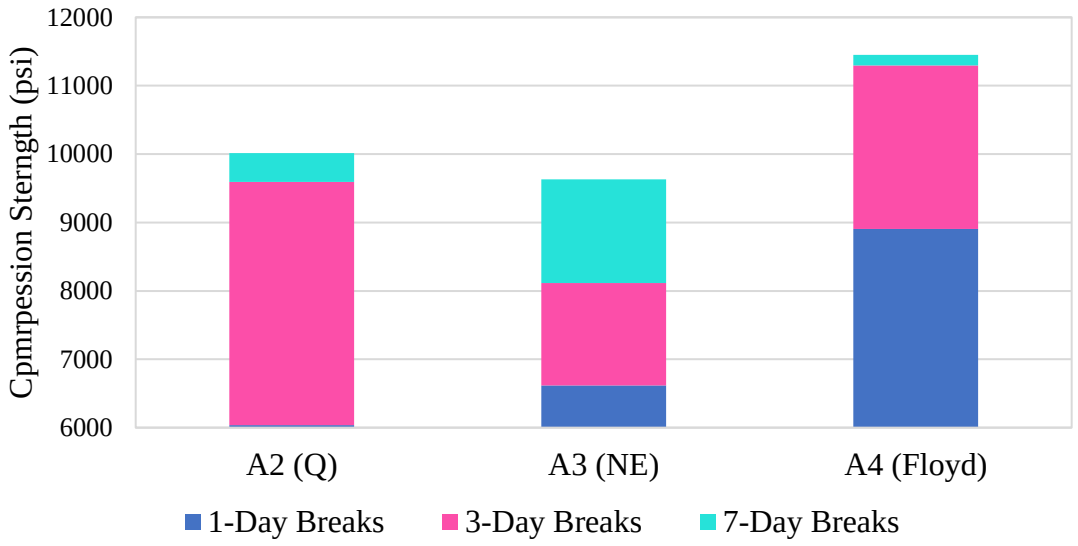

Figure 3.4 Compressive Strengths of Baseline Series A

While the "Floyd" mix had the highest compressive strength, the mixture was untenable; it was sticky, viscous, and could not be poured. The Graybeal NE had the highest compressive strength of the two with a workable texture and was chosen as the baseline for the rest of Series A. A broad set of parameters were then tested, with the expectation that more thorough studies would be conducted on the parameters that proved to be of interest. The parameters varied were w/cm ratio, aggregate/cementitious material ratio, and the amount and type of SCM replacement. These mix designs are shown in Table 3.3. The compressive strength results are shown in Figure 3.5.

Table 3.3 Series A Mix Design Proportions

	A2	**A3**	**A4**	**A5**	**A6**	**A7**	**A8**	**A9**	**A10**
Type III Cement	0.70	0.70	0.75	0.70	0.70	0.70	0.70	0.70	0.70
Silica Fume	0.15	0.15	0.15	0.15	0.15	0.15	0.15	0.15	0.15
Fly Ash	0.15	0.15	0.1	0.15	0.15	0.15	0.15	0.15	0.15
w/cm	0.23	0.23	0.18	0.23	0.23	0.23	0.22	0.21	0.20
agg/cm	1.00	1.00	0.75	1.00	1.00	1.00	1.00	1.00	1.00
HRWR (oz./cwt)	21.0	22.0	22.0	18.7	21.0	16.3	18.7	18.7	18.7

	A11	A12	A13	A14	A15	A16	A17	A18	A19
Type III Cement	0.70	0.70	0.70	0.75	0.70	0.70	0.70	0.73	0.75
Silica Fume	0.15	0.15	0.15	0.20	0.20	0.15	0.15	0.14	0.13
Fly Ash	0.15	0.15	0.15	0.05	0.10	0.15	0.15	0.13	0.12
w/cm	0.23	0.23	0.23	0.23	0.23	0.23	0.23	0.23	0.23
agg/cm	0.90	0.80	0.70	1.00	1.00	1.00	1.00	1.00	1.00
HRWR (oz./cwt)	18.7	18.7	18.7	18.7	18.7	18.7	18.7	18.7	18.7

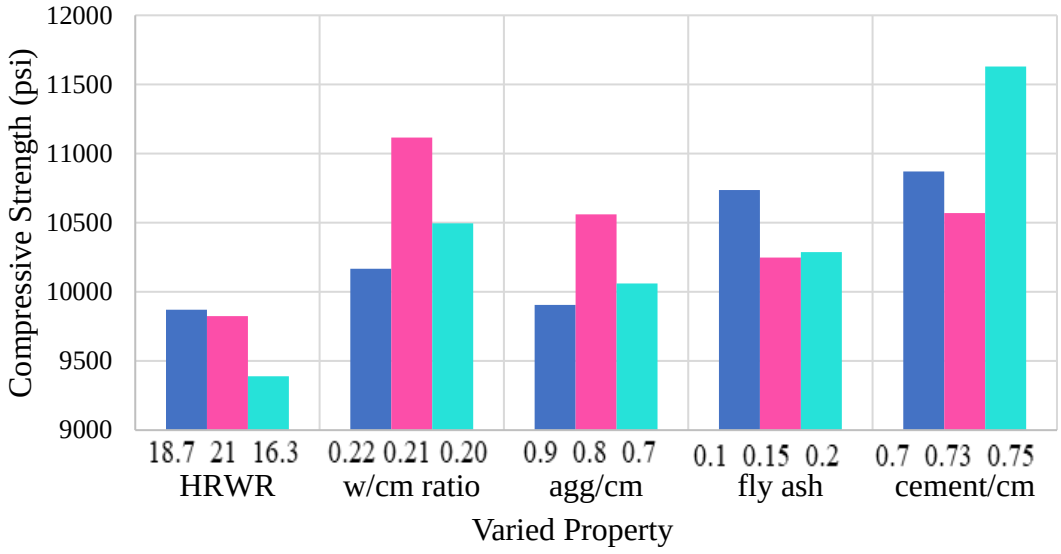

Figure 3.5 Compressive Strengths of Series A

While the results of this series were used to continue the iterative process, this study highlighted several sources of error which were addressed before continuing the investigation. There were sources of error recognized in the first step of this experiment, both correlated with the mortar flow and texture. The bubbles that formed at the top of the cubes varied significantly between mixes, with increased mortar flow correlating with more bubbles. Additionally, tested cubes showed small bubble-sized voids. The frequency of the voids caused the texture of the interior of the cubes to range from large infrequent voids to a porous honeycomb structure. Mixes with high mortar flow

correlated with dense interiors, with several small bubbles. Lower mortar flow mixes correlated with fewer, larger voids. While these correlations were observed, there was a concern that variations in consolidation procedure led to the differences in the interior structure and finished surface.

The mixes with reduced mortar flow, particularly those mixes with mortar flows of less than 6 in., "stuck" to the greased molds, leaving a rough surface that was sanded off with a pumice stone to provide a smooth surface on which to break in the testing machine. Mixes with very high mortar flow would flow out and under cube molds, so the corners of the cube were sanded with pumice to ensure even contact with the testing apparatus. However, "smooth" is an objective measure, and differed slightly among the operators.

An experiment was conducted to determine whether this was an inherent property of UHPC mixes, which should not be controlled for, or an inconsistency in the production method. To study the difference in microstructure due to consolidation, a mix with the then-target flow of 10 in. was selected. This batch was mixed according to the procedure described earlier. Immediately after the end of the mixing time, the first specimens were poured into their molds; 3 specimens were taken immediately to the curing chamber, and 3 were tapped 25 times on each side of the mold for a total of 50 taps. The bowl was then moved to the vibration table.

The bowl rested on the vibrating bottom of the table and was loosely braced a foot off the vibration table with a section of plywood. The table was vibrated for a specified period of time. The vibrator was turned off, and specimens were cast from the bowl sitting on the vibration table. The vibrator was then turned back on to vibrate

specimens for additional time, until the next time of interest was reached. The time and results reported were compounded in this way. Batches were made to test the results of vibration at both low and high frequencies. The visual results of the test are shown in Figures 3.6 and 3.7.

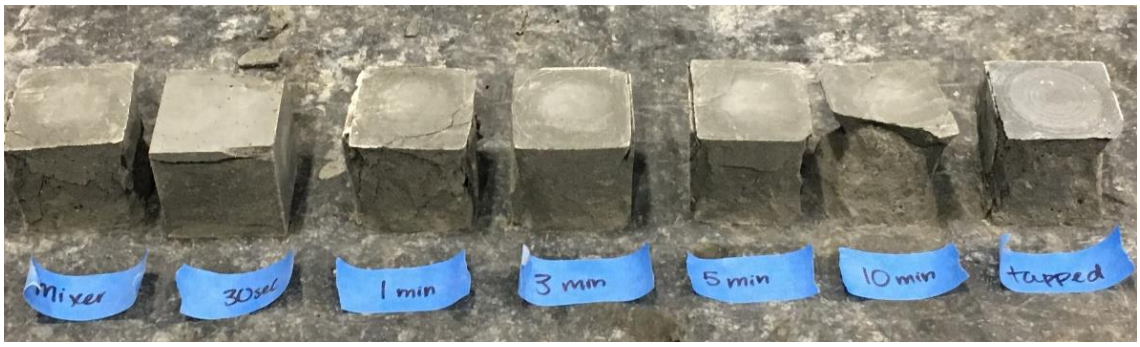

Figure 3.6 Consolidation of Mortar Cubes After Low-Frequency Vibration

Figure 3.7 Consolidation of Mortar Cubes After High-Frequency Vibration

The photographs shown in Figures 3.6 and 3.7 were taken after the specimens had been broken in compression and show obvious changes in the internal structure as the time of vibrations is increased. The cubes taken straight out of the mixer show a honeycomb of small, discontinuous bubbles within the mix. The frequency of these bubbles decrease steadily as the level of vibration is increased. There is not much visual difference in the consolidation between the 5 and 10-minute intervals for the low frequency and for the 3 and 5-minute intervals for the high frequency, though the graph

in Figure 3.8 shows that there were strength gains between these intervals.

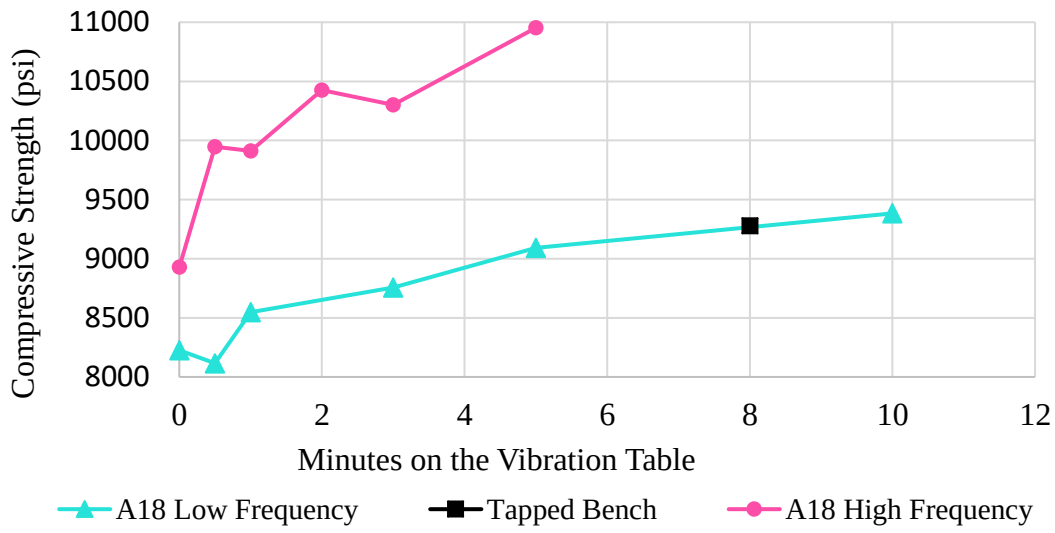

Figure 3.8 Compressive Strengths at Different Levels of Vibration

Both the low and high frequency vibration schemes showed increased strength correlated with increased time on the vibration table. However, the control batches of these mixes varied significantly in their strength. The source of this discrepancy is unknown, and the efficacy of the bench vibration frequency could not be compared directly. However, a direct comparison can be made between the tapped bench specimen and the low frequency table specimens. The tapped bench specimens were comparable to the specimens vibrated at low frequency for 8 minutes.

Tapping the bench was chosen to be the standard used for the rest of the mix design process. While the paste could have been vibrated further, it would not be practical. Steel fibers would inevitably be added to the ideal concrete paste, and these fibers would align and settle if over consolidated or vibrated (Graybeal, 2006). Therefore, it would not be useful to fully consolidate the air bubbles out of the specimens, given that these bubbles would be retained in the final version of these

mixes. However, previous experience with the mixes showed that no or poorly executed consolidation resulted in large holes in the sides and corners of cubes. Tapping on the bench was chosen as the future method of consolidation as it provided consistent results, while hopefully retaining a representative amount of air.

The next set of tests was conducted on a set of cubes consolidated by bench tapping. This study investigated the surface preparation method for the cube specimens. The cubes were scratched in three ways: on the corners of the breaking surface, in perpendicular scratches across the entire breaking surface with pumice stone, and excess concrete and roughness taken off with one pass of a pallet knife, with the results shown in Figure 3.9.

Figure 3.9 Mortar Cube Surface Preparation

These cubes were tested in compression, and the results are shown in Figure 3.10. The pallet-knife scraped cubes performed slightly better than the other two methods. More significantly, the cube fracture patterns were more consistent (with a smaller standard deviation) with the pallet-knife scraped sides than the other methods. The pallet knife scraping could also be employed more consistently than the other methods, given that the number of scrapes could be clearly defined.

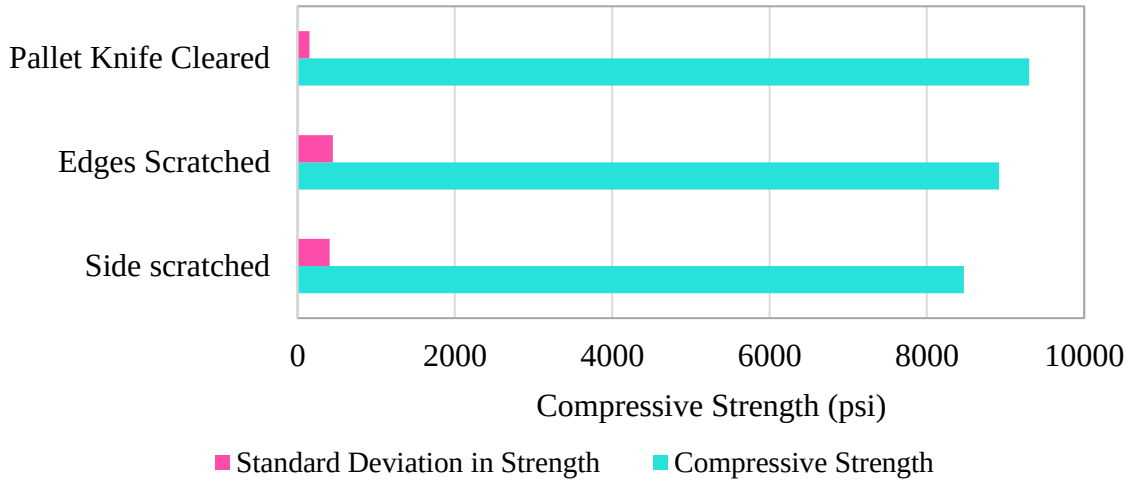

Figure 3.10 Difference in Compressive Strength Due to Surface Preparation

After these studies, it was concluded that further series would be cleaned with a pallet knife and consolidated with 50 taps on the bench. Additionally, it was decided that mixes with mortar flow less than 6 inches would be tamped in the manner specified in ASTM C109.

Series A sought to establish a mix design baseline with a workable texture, a mortar flow in the target range, and a high compressive strength. The mix A19 met these requirements, and had the highest 7-day compressive strength of the Series at 11,630 psi. Additionally, this Series indicated that air content was a key factor in the performance of the mixes.

3.4 Series B: Establishing Optimal Water/HRWR/Cement Proportions

This series investigated the relationship between water and HRWR. Finding the optimal w/cm ratio is critical, as it defines how much of the cementitious material becomes hydrated and what portion is simply used as filler. The w/HRWR ratio is also critical, as the HRWR has a significant impact on the texture of the mix.

The baseline mix established in the last Series, A19, showed flecks of unused HRWR floating on the top of the concrete after mixing was complete, as shown in Figure 3.11. These visible flecks of HRWR could also be seen floating on the top of batched specimens.

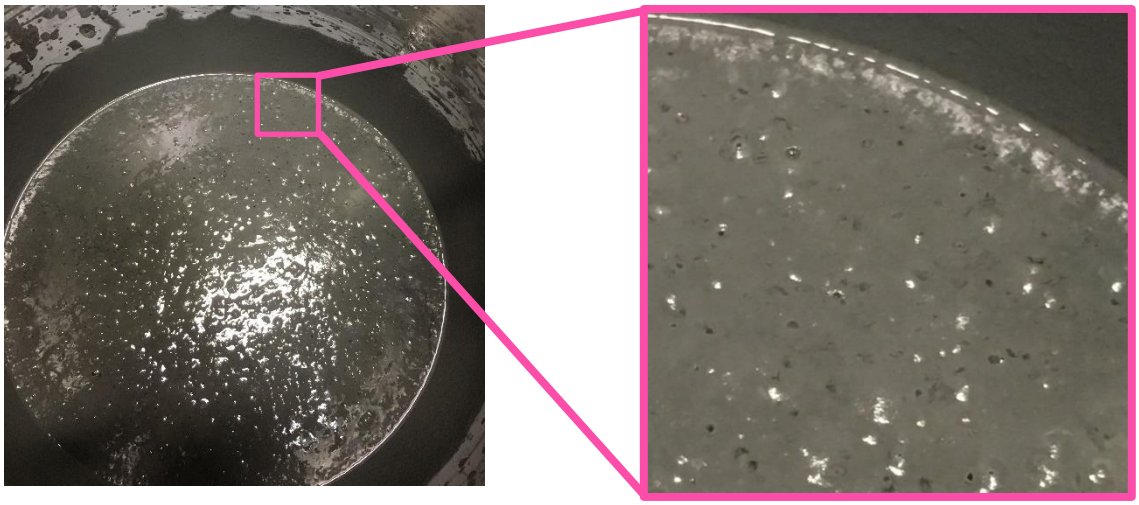

Figure 3.11 Floating Specks of Unused HRWR

Unused HRWR is a problem, because it is significantly weaker than anything else in the concrete except air. If the HRWR rises to the top quickly enough, it would be a problem that was ultimately addressed in the implementation phase of the project, through grinding of the top surface, which would eliminate the weaker material containing the unused HRWR and excessive air bubbles. However, there is not an obvious way to measure how much HRWR floated or insure that all the unused HRWR floated to the surface. To address this issue, a mix design scheme was implemented to find the optimal w/HRWR and w/cm ratio, Series B, which is shown in Table 3.4.

Table 3.4 Series B Mix Design Proportions

	B1	B2	B3	B4	B5	B6	B7	B8	B9
Type III Cement	0.75	0.75	0.75	0.75	0.75	0.75	0.75	0.75	0.75
Silica Fume	0.125	0.125	0.125	0.125	0.125	0.125	0.125	0.125	0.125
Fly Ash	0.125	0.125	0.125	0.125	0.125	0.125	0.125	0.125	0.125
w/cm	0.2	0.19	0.18	0.23	0.23	0.23	0.19	0.19	0.19
agg/cm	1.00	1.00	1.00	1.00	1.00	1.00	1.00	1.00	1.00
HRWR (oz./cwt)	18.7	18.7	18.7	16.3	14.0	11.67	21.0	23.33	25.66

The results of this series in terms of mortar flow are given in Figure 3.12. The increasing size of the dot indicates an increasing amount of HRWR.

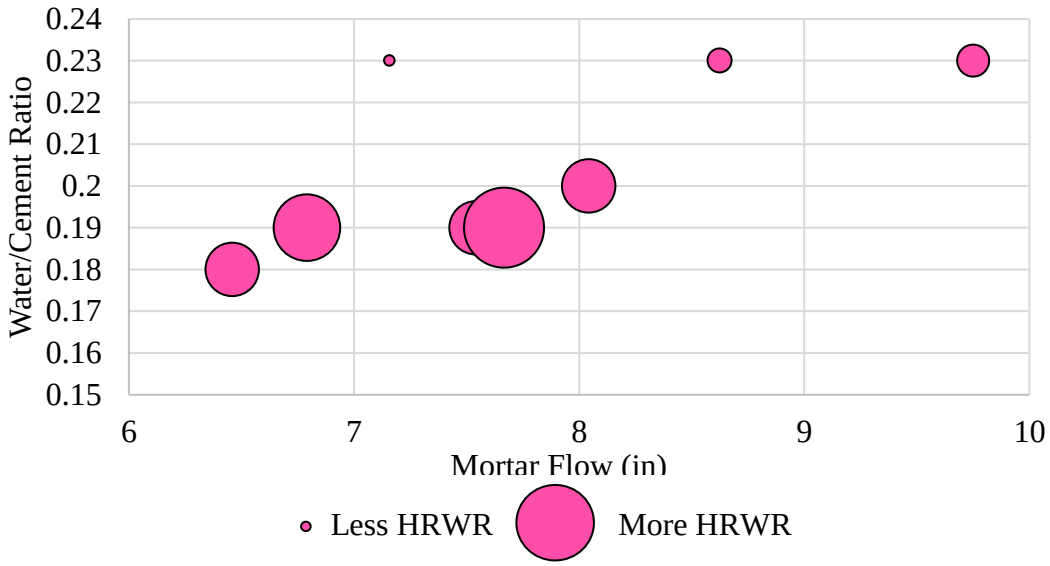

Figure 3.12 Water/Cementitious Material Ratio vs. Mortar Flow

Figure 3.12 shows that the HRWR increases mortar flow at the same w/cm ratio. However, the increase of HRWR is not as influential on the mortar flow as the w/cm ratio. Except for the mix that had the lowest dosage of HRWR, B6, an increase of w/cm led to an increase in mortar flow.

Although the mortar flow is one of the targets of this study, the most essential property is strength. The relationship between the mortar flow and compressive strength for this series is shown in Figure 3.13.

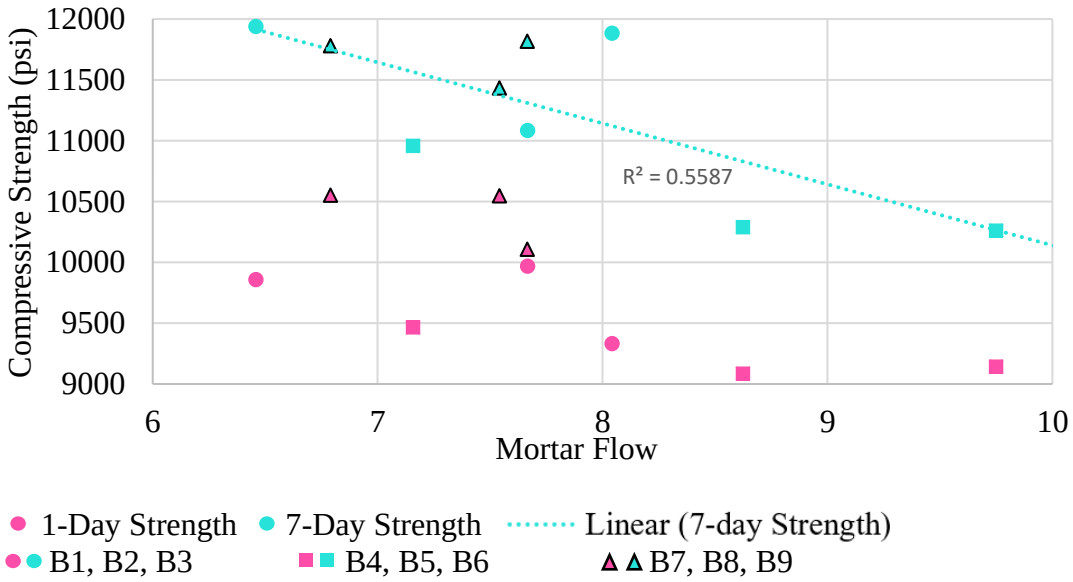

Figure 3.13 Mortar Flow vs. Compressive Strength

Figure 3.13 displays the general trend that the greater the mortar flow, the less compressive strength the mix exhibited. However, the correlation between compressive strength and mortar flow is weak, and with an R-value less than 0.6, the correlation is not compelling. There are multiple factors displayed here as well. The highest w/cm tested, 0.23 (shown in the above graph as squares) showed the lowest strengths, and the lower w/cm ratios, 0.18-0.20, showed comparable strengths.

The most optimal combination of HRWR and w/cm ratio was found in B1, with a HRWR dosage of 18.7 and a w/cm ratio of 0.2. While B3, a mix with the same HRWR but a w/cm ratio of 0.18 was slightly stronger (11,940 psi vs. 11,880 psi), the mixture was sticky and had poor mortar flow. This study showed that a tenable

consistency was not achievable with lower w/cm ratio, as the amount of HRWR required to compensate for the reduction in mortar flow caused the mixture to become sticky and unworkable.

3.5 Series C: Introducing Supplementary Cementitious Materials

Series C sought to investigate the effect of varying the types and amount of SCMs. Certain SCMs are suggested in the literature to achieve high compressive strengths, both by increasing particle packing and adding later pozzolanic reactions (Ibrahim et al., 2013). While not a direct consideration for this research, replacing a high carbon production product like cement with industrial byproducts, such as GGBFS, fly ash, and silica fume, benefits the environment (Radlinkski et al., 2011). The mixes of Series C varied the amount of established SCMs, as well as integrating additional GGBFS and Type I cement. The Series C mix designs are shown in Table 3.5.

Table 3.5 Series C Mix Design Proportions

	C1	**C2**	**C3**	**C4**	**C5**	**C6**	**C7**	**C8**
Type III Cement	0.7	0.65	0.6	0.825	0.775	0.725	0.825	0.775
Silica Fume	0.125	0.125	0.125	0.05	0.1	0.15	0.125	0.125
VCAS ™	0	0	0	0	0	0	0	0
Fly Ash	0.125	0.125	0.125	0.125	0.125	0.125	0.05	0.1
GGBFS	0	0	0	0	0	0	0	0
Type I Cement	0.05	0.1	0.15	0	0	0	0	0
w/cm	0.20	0.20	0.20	0.20	0.20	0.20	0.20	0.20
agg/cm	1.00	1.00	1.00	1.00	1.00	1.00	1.00	1.00
HRWR (oz/cwt)	18.7	18.7	18.7	18.7	18.7	18.7	18.7	18.7

	C9	C10	C11	C12	C13	C14	C15	C16
Type III Cement	0.725	0.7	0.65	0.6	0.7	0.65	0.6	0.65
Silica Fume	0.125	0.125	0.125	0.125	0.125	0.125	0.125	0.05
VCAS ™	0	0	0	0	0.05	0.1	0.15	0
Fly Ash	0.15	0.125	0.125	0.125	0.125	0.125	0.125	0.1
GGBFS	0	0.05	0.1	0.15	0	0	0	0
Type I Cement	0	0	0	0	0	0	0	0.2
w/cm	0.20	0.20	0.20	0.20	0.20	0.20	0.20	0.20
agg/cm	1.00	1.00	1.00	1.00	1.00	1.00	1.00	1.00
HRWR (oz/cwt)	18.7	18.7	18.7	18.7	18.7	18.7	18.7	18.7

	C17	C18	C19	C20	C21	C22	C23	C24
Type III Cement	0.55	0.45	0.8	0.75	0.7	0.85	0.8	0.75
Silica Fume	0.05	0.05	0.1	0.15	0.2	0.05	0.05	0.05
VCAS ™	0	0	0	0	0	0	0	0
Fly Ash	0.1	0.1	0.1	0.1	0.1	0.1	0.15	0.2
GGBFS	0	0	0	0	0	0	0	0
Type I Cement	0.3	0.4	0	0	0	0	0	0
w/cm	0.20	0.20	0.20	0.20	0.20	0.20	0.20	0.20
agg/cm	1.00	1.00	1.00	1.00	1.00	1.00	1.00	1.00
HRWR (oz/cwt)	18.7	18.7	18.7	18.7	18.7	18.7	18.7	18.7

To attempt to understand the effect of the individual SCMs on compressive strength, the portion of SCM replacement was considered in isolation of the other constituents, as shown in Figure 3.14. It is evident from the results in Figure 3.14 that considering the effect of an individual SCM is not useful. There is not a strong correlation between any particular portion of SCM and strength. The exception was the fly ash, which featured a strong negative correlation with increasing levels of replacement. However, there is sufficient scatter across the data that even this conclusion is not compelling.

Series A and B featured silica fume and Type III cement, which gain strength early. The only SCM in these mixes that retard strength gain was fly ash, and the

maximum replacement was 20%. For these reasons, 7 days was a reasonable time frame to assess ultimate strength. However, Series C has high levels of SCMs and Type I cement, which gain strength more slowly. Breaks at 28-days were phased in during this series as a more appropriate assessment of ultimate strength to compare with these earlier values. A misalignment in the compressive testing machine that lasted several days left some patches of unreliable data. These unreliable data points are reported in the appendix, but not in Figure 3.14, which is a summary of the effect of SCMs on the 28-day compressive strength.

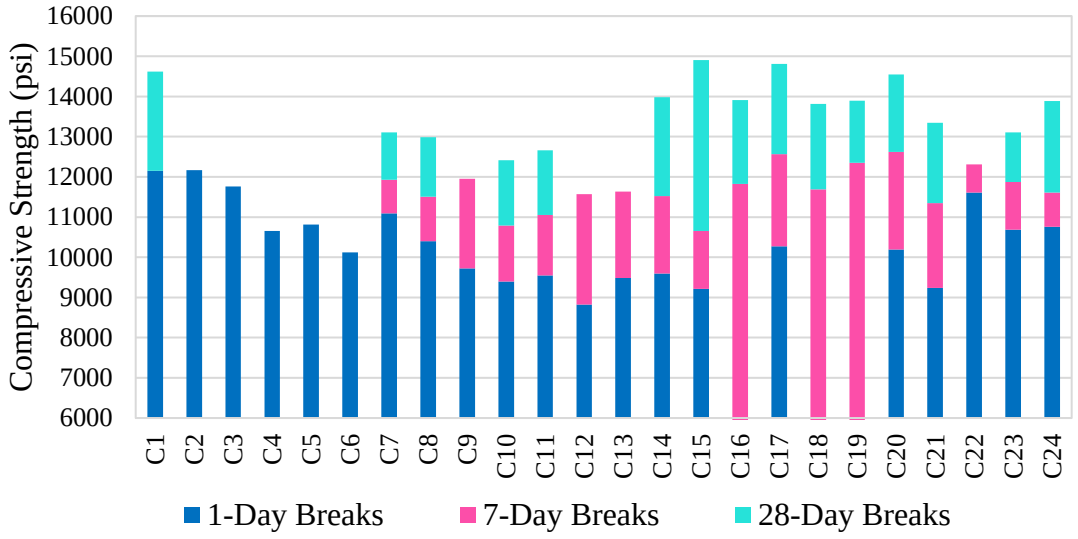

Figure 3.14 Effect of SCMs on 28-Day Compressive Strength

Given that the primary cement used in Series C is Type III, there was not an expectation of a significant strength increase between 7 and 28 days. However, the 28-day compressive strengths confirmed that the mixes of Series C and prior fell short of the final target strength of 22 ksi. The magnitude of the shortfall indicated that a different strategy might need to be employed to reach target strengths.

This study resulted in several promising mixes, including C1, C15, C17, and C20, which all had compressive strengths at 28 days exceeding 14,500 psi. There is not a greater pattern to be discerned from these mixes; they had no amount of any constituent in common. There was not a common cement/cementitious ratio that seemed advantageous. It was learned that very particular chemical combinations may not show trends with similar combinations. C15 and C17 were chosen to use in future iterations, given their combination of high strengths, mortar flow, and workable texture.

3.6 Series D: Optimal Particle Packing Mixes

Results short of the target demanded a new strategy to reach the compressive strength goals of the project. A theoretical approach was to be used in conjunction with the experimental approach to achieve a mix with near-optimal particle packing, which literature indicates can lead to increased strength (Fennis and Walraven, 2012; Kim et al., 2016).

In this experiment, the Modified Andersean and Anderson Model was used to create the optimal particle packing curve. This model, developed by Funk and Dinger in 1994, was preferred over the original Andersean and Anderson model because it uses both the minimum and maximum aggregate size to formulate the optimal curve (1994). The original model was developed for mixes with more typical coarse and fine aggregate sizes and does not accommodate the majority of particles condensed in a compact gradation. This Modified model, shown as Eq. 3.1, was developed to accommodate the finer particles,

$$D(P) = \frac{D^q - D_{min}^q}{D_{max}^q - D_{min}^q} \qquad \text{(Eq. 3.1)}$$

where *D(P)* outputs the percent passing each diameter at the optimal packing curve, D^q is the diameter (the sieve size in a typical analysis) of interest, D_{min}^q is the minimum particle size of the constituents used in the mix, and D_{max}^q is the maximum particle size of the constituents used in the mix.

The literature does not indicate a consensus for the optimal q-value, as discussed in the literature review. A q-value of 0.22 was chosen because it fell within the recommended range for several parameters, including flowability and high strength for fine-particle dominant mixes (Kim et al., 2016; Sbia et al., 2016; Ye et al.,2012). This value also fell within the recommended range of the EMMA software program for high strength, fine-particle dominant mixes.

This model used the gradations found by the Beckman Coulter particle analyzer. The optimal particle packing curve with the q-value of 0.22 is presented in Figure 3.15, with the gradations of the UHPC constituents for context.

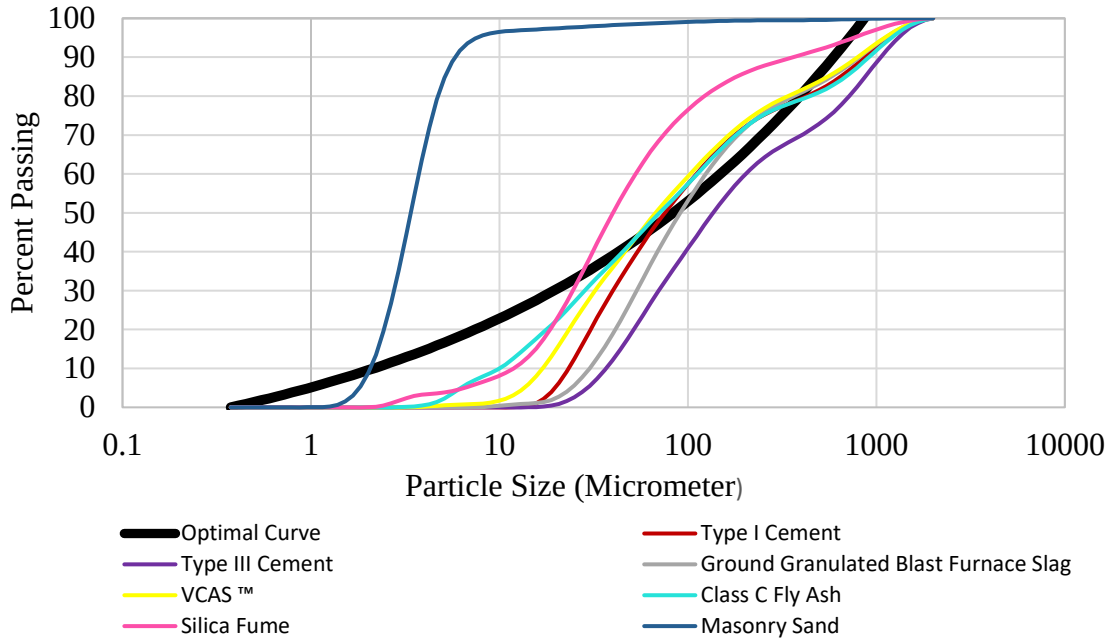

Figure 3.15 Optimal Particle Packing Curve for UHPC

The intention of the study was to use the EMMA software to optimize particle packing. Unfortunately, the output of the EMMA software is strictly graphical, as shown in Figure 3.16. While this output could be used to compare the particle packing of existing mixes, there was not an effective way to generate mixes using this software.

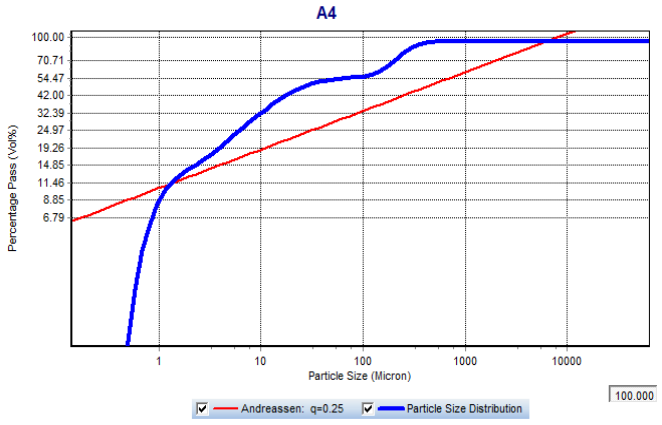

Figure 3.16 EMMA Output of Mix A4

A comprehensive analysis of particle packing was instead conducted with an Excel spreadsheet. To directly compare mixes, an "error" value was produced for each mix. This "error" value was found using the RSS method. A weighted average of the concrete constituents was tabulated for each point of gradation. The value of the distance from the total mix gradation to the optimal curve is squared at each point of gradation. This squared value is added across every gradation point, so that a single value represents the error over the entire curve. This value was divided by 1000 to make the numbers easier to read at a glance.

This analysis included 17,600 potential mixes, though not all were viable. There were several matrices constructed to ensure all possible mixes with the given constituents were analyzed. The first varied silica fume and fly ash in 5% increments up to 50% total cementitious material replacement, with the remainder of cementitious materials designated Type III cement. Silica fume was studied in every matrix because the uniquely small particle size is the only constituent that could fill in the bottom of the optimal packing curve (Graybeal, 2013). Cement is obviously necessary, as pozzolans rely on the first cementitious reaction to activate. The second matrix considered the interaction between silica fume, fly ash, and GGBFS, the remainder designated Type III cement. Given that levels of replacement were explored to 50% for each SCM, there is a portion of mixes that have negative portions of cement. These potential mixes were ignored. The third matrix considered the combination of silica fume, fly ash, VCAS™, and Type I cement. The fourth considered silica fume, fly ash, and Type I cement. The fifth matrix considered the combination of 0-50% replacement of silica fume and fly ash with 0-100% replacement of Type III cement, and the remainder of each mix

designated Type I. These five matrices were developed for aggregate/cementitious material ratios of 1.0, 1.1, 0.9, and 0.8. A portion of a matrix with the aggregate/cementitious material ratio of 1.0 is provided in Table 3.6 as a sample.

Table 3.6 Sample Portion of RSS Matrix

Type III	0.65	0.6	0.55	0.5	0.45	0.4	0.35	0.3	0.25	0.2	0.15
Silica Fume	0.2	0.2	0.2	0.2	0.2	0.2	0.2	0.2	0.2	0.2	0.2
Fly Ash	0	0.05	0.1	0.15	0.2	0.25	0.3	0.35	0.4	0.45	0.5
GGBFS	0	0	0	0	0	0	0	0	0	0	0
Type I	0.15	0.15	0.15	0.15	0.15	0.15	0.15	0.15	0.15	0.15	0.15
VCAS	0	0	0	0	0	0	0	0	0	0	0
RSS	3.8444	3.6203	3.4136	3.2245	3.0528	2.8987	2.762	2.6428	2.5412	2.457	2.3903
Type III	0.6	0.55	0.5	0.45	0.4	0.35	0.3	0.25	0.2	0.15	0.1
Silica Fume	0.2	0.2	0.2	0.2	0.2	0.2	0.2	0.2	0.2	0.2	0.2
Fly Ash	0	0.05	0.1	0.15	0.2	0.25	0.3	0.35	0.4	0.45	0.5
GGBFS	0	0	0	0	0	0	0	0	0	0	0
Type I	0.2	0.2	0.2	0.2	0.2	0.2	0.2	0.2	0.2	0.2	0.2
VCAS	0	0	0	0	0	0	0	0	0	0	0
RSS	3.7044	3.4915	3.2962	3.1183	2.9579	2.815	2.6896	2.5817	2.4913	2.4183	2.3629

The most obvious generality observed is that the most optimal particle packing mixes occurs at the aggregate/cementitious material ratio of 1.0, followed by 1.1, 0.9, then 0.8. Table 3.7 provides the limits of each matrix.

Table 3.7 Limits of Each Particle Packing Matrix

	Aggregate/ Cementitious Material Ratio							
	0.8		0.9		1		1.1	
	RSS (Error from Ideal Particle Packing Curve)							
	max	min	max	min	max	min	max	min
Type III +SF+FA	29.959	13.867	25.140	10.330	5.986	2.309	18.170	7.817
+ GGBFS	29.000	12.882	24.354	10.631	5.614	2.366	17.566	7.586
+VCAS	28.504	13.532	23.958	11.215	5.460	2.296	17.270	7.812
+ Type I	28.786	13.168	24.169	11.088	5.565	2.361	17.426	7.829
Overall	29.959	12.882	25.140	10.330	5.986	2.296	18.170	7.586

The poorest particle packing, or highest RSS value, falls in the same location in every matrix for every aggregate/cementitious material ratio. The highest RSS mix in every matrix is 5% replacement of silica fume and 5% other SCM. However, there are differences between the aggregate/cementitious material ratio in the location of the minimum RSS value within each matrix. Mixes with higher levels of silica fume have better particle packing when all else is held constant. The relative RSS values make similar patterns between each aggregate/cementitious material ratio, with the same groups consistently touting the lowest RSS values. The best particle packing group in each matrix is provided below for the aggregate/cementitious material ratio case of 1.0. The groups shown in Table 3.8 are the same for other ratios, but will have different RSS values.

Table 3.8 Groups of Mixes with the Best Particle Packing Potential

		Portion of Type III Cement Replacement			
Groups of Mixes with Highest Particle Packing	Silica Fume	0.35- 0.4	0.15- 0.30	0.3- 0.4	0.15- 0.20
	Fly Ash	0.35- 0.5	0.25- 0.50	0.25-.0.5	0.00- 0.05
	GGBFS			0.05- 0.35	
	VCAS				0.05- 0.10
	Type I Cement		0.10- 0.35		
RSS Range		2.309- 2.330	2.309- 2.375	2.319- 2.518	3.556- 3.974

The three mixes with the best particle packing were selected for the first round of mixing. The next eight mixes were selected from the mixes that had at least 60% combined Type I and Type III cement. The rest of the mixes in the series increased the replacement of VCAS™ and Type III, to increase the packing potential of mixes in Series C that showed the most promise, C13 and C15. These mix designs are provided

in Table 3.9.

Table 3.9 Series D Mix Design Proportions

	D1	D2	D3	D4	D5	D6	D7	D8	D9	D10	D11
RSS	2.309	2.315	2.309	2.672	2.666	2.670	2.654	2.647	2.653	2.636	2.628
Type III Cement	0.15	0.1	0.05	0.1	0.1	0.05	0.05	0.05	0	0	0
Silica Fume	0.35	0.35	0.35	0.25	0.3	0.15	0.2	0.25	0.1	0.15	0.2
VCAS ™	0	0	0	0	0	0	0	0	0	0	0
Fly Ash	0.5	0.5	0.5	0.05	0	0.15	0.1	0.05	0.2	0.15	0.1
Type I Cement	0	0.05	0.1	0.6	0.6	0.65	0.65	0.65	0.7	0.7	0.7
w/cm	0.2	0.2	0.2	0.2	0.2	0.2	0.2	0.2	0.2	0.2	0.2
agg/cm	1.00	1.00	1.00	1.00	1.00	1.00	1.00	1.00	1.00	1.00	1.00
HRWR (oz./cwt)	18.7	18.7	18.7	18.7	18.7	18.7	18.7	18.7	18.7	18.7	18.7

	D12	D13	D14	D15	D16	D17
RSS						
Type III Cement	0.55	0.5	0.45	0.6	0.5	0.45
Silica Fume	0.125	0.125	0.125	0.05	0.05	0.125
VCAS ™	0.2	0.25	0.3	0	0	0
Fly Ash	0.125	0.125	0.125	0.1	0.1	0.125
Type I Cement	0	0	0	0.25	0.35	0.3
w/cm	0.2	0.2	0.2	0.2	0.2	0.2
agg/cm	1.00	1.00	1.00	1.00	1.00	1.00
HRWR (oz./cwt)	18.7	18.7	18.7	18.7	18.7	18.7

Testing revealed that the best particle packing mixes were not viable. With the same water and HRWR used for previous mixes, the mix never “broke.” There are several stages in the mixing process. First, the water begins to suspend in the mixture, and coarse crumbs are formed. These crumbs then begin to stick together to form several large clumps of concrete. At this stage, the mixer’s motor becomes audible, and

the mixer gently rocks as the consolidated weight of the concrete is pushed from one side of the bowl to the other. Most mixes at this point "break." The HRWR and water have been suspended, the mixture slackens, and the mixer stops rocking. Every mix follows this pattern, but only mixes with mortar flows exceeding around 5 inches ever break, or fall into a slump.

None of the three best particle packing mixes broke, even given extra mixing time at the highest shear setting. The high level of silica fume, which has a very large specific surface, could be the cause of this behavior. Cubes could not be consolidated, as the mixture stuck to the tamper and could not be pressed into the bottom of the mold, as shown in Figure 3.17. The strengths of these cubes could not be accurately determined because of this poor consolidation.

Figure 3.17 Unconsolidated Cubes of Mix D1 and D2

The next set of mixes (D4-D11) were selected for the best particle packing, with the additional qualifier that the total amount of cement, Type I and III combined, reached 60% of the total cementitious material. This is the minimum amount of cement that had been tested in previous series. While several of these mixes had mortar flows less than 6 in. and had to be tamped, they were not too sticky to consolidate properly, and all broke during mixing. The next set of mixes (D12-D17) made improvements on

the best mixes of the previous series (C13, C15) by making changes that would improve the particle packing. The mortar flow and the compressive strengths of the cubes as a function of the RSS are displayed in Figures 3.18 and 3.19, respectively.

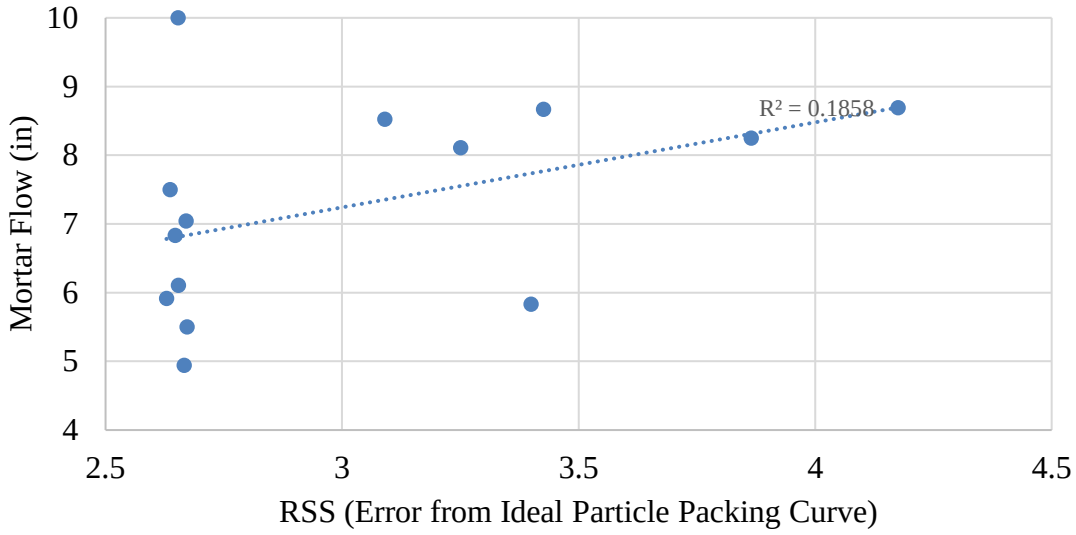

Figure 3.18 RSS vs. Mortar Flow

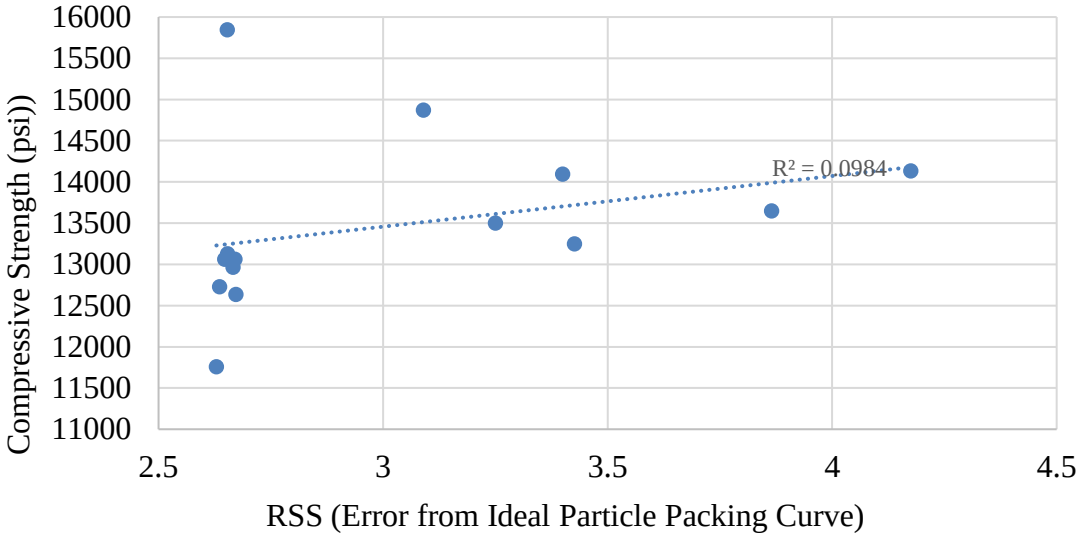

Figure 3.19 RSS vs. Compressive Strength

As seen from the graphs, there is no correlation between either RSS error and mortar flow or RSS error and compressive strength. However, there are mixes in Series D that show superior compressive strength compared to the mixes of previous series. The compressive strengths of Series D are shown in Figure 3.20.

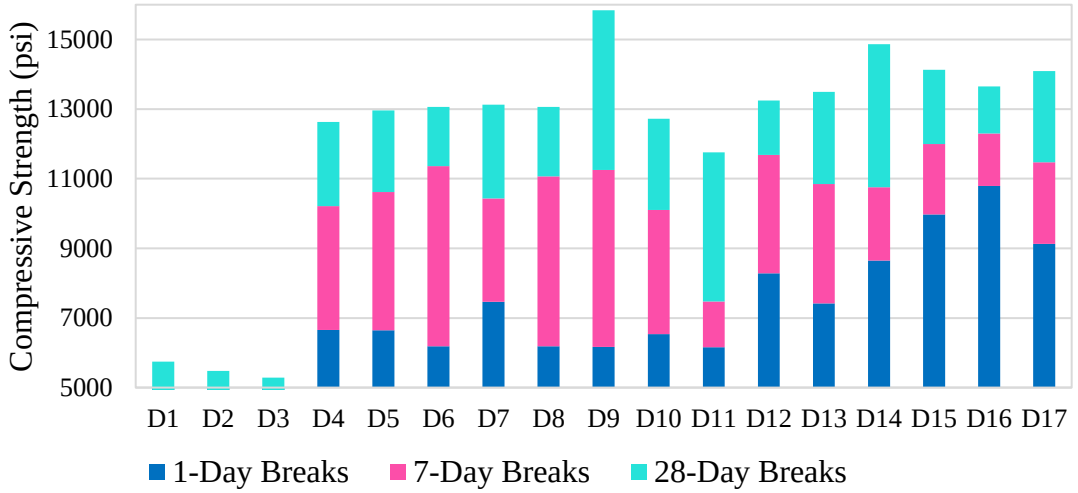

Figure 3.20 Compressive Strength of Series D

This series did not provide any insight in how to develop UHPC based on exclusively particle packing. The chemical compatibility of these constituents proved more significant than the physical compatibility. Only two mixes, D9 and D14, have compressive strengths comparable or better than mixes C15 and C17 at 15,840 psi and 14,870 psi, respectively.

3.7 Series E: Effects and Benefits of Type I vs. Type III Cement

The previous mixes in this series displayed some correlation that mixes with higher proportions of Type I cement had higher mortar flow compared to mixes with higher proportions of Type III cement. Type III cement and Type I cement should have

the same 28-day strength, with Type III cement achieving that strength much earlier, at about 7 days.

To investigate how combinations of Type I and Type III cements affect the mortar flow and the timetable of strength gain, a study of exclusively these cements was conducted. This series, shown in Table 3.10, varied Type I and Type III replacements between zero to 100%.

Table 3.10 Series E Mix Design Proportions

	E1	**E2**	**E3**	**E4**	**E5**	**E6**	**E7**
Type III Cement	0	0.1	0.15	0.2	0.25	0.3	0.35
Type I Cement	1	0.9	0.85	0.8	0.75	0.7	0.65
w/cm	0.2	0.2	0.2	0.2	0.2	0.2	0.2
cm/agg	1.00	1.00	1.00	1.00	1.00	1.00	1.00
HRWR (oz/cwt)	18.70	18.70	18.70	18.70	18.70	18.70	18.70
Mortar Flow (in)	9.75	9.5	9	8.917	8.775	8.717	5.442

	E8	**E9**	**E10**	**E11**	**E12**	**E13**	**E14**	**E15**
Type III Cement	0.4	0.45	0.5	0.6	0.7	0.8	0.9	1
Type I Cement	0.6	0.55	0.5	0.4	0.3	0.2	0.1	0
w/cm	0.2	0.2	0.2	0.2	0.2	0.2	0.2	0.2
cm/agg	1.00	1.00	1.00	1.00	1.00	1.00	1.00	1.00
HRWR (oz/cwt)	18.70	18.70	18.70	18.70	18.70	18.70	18.70	18.70
Mortar Flow (in)	7.583	7.917	7.167	5.333	5.833	5.667	5.75	4.917

The results of this experiment are shown in Figure 3.21 for mortar flow and Figure 3.22 for compressive strength as a function of the proportion of Type I cement. As shown in Figure 3.21, it is evident that increasing amounts of Type I cement directly lead to increased mortar flow, except for an outlying point identified in an outlier analysis. This result is most likely due to the increased fineness and thus surface area of

Type III cement, which increases the water demand compared to Type I cement.

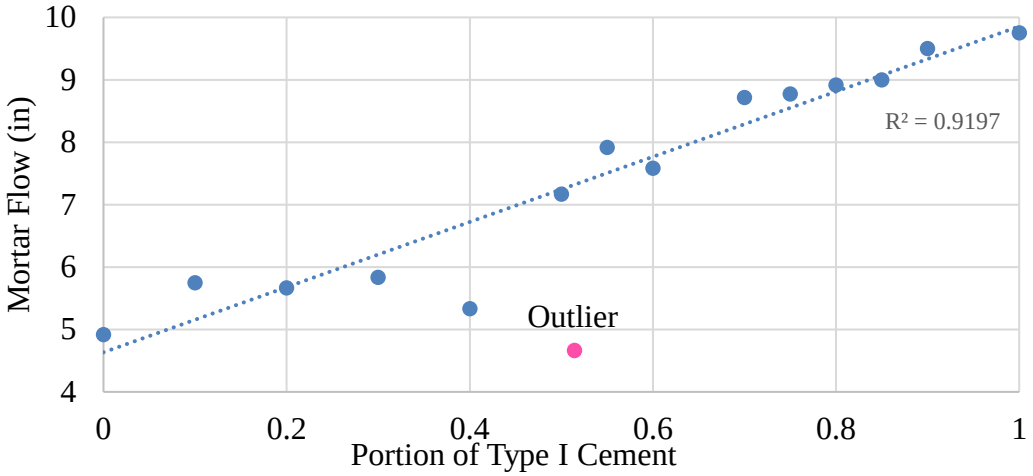

Figure 3.21 Proportion of Type I Cement vs. Mortar Flow

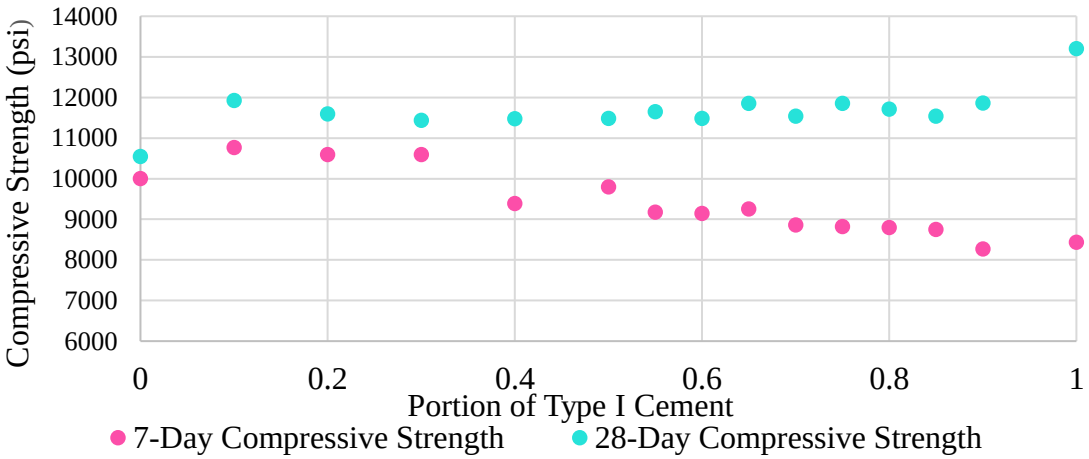

Figure 3.22 Proportion of Type I Cement vs. Compressive Strength

Increased proportions of Type III cement showed increases in 7-day compressive strengths, as shown in Figure 3.22. The 28-day strengths are similar for all combinations of Type I and Type III cements, except for 0% and 100% Type I, where there was a marked drop-of, and slight bump, respectively. There does not seem to be any combination of the two cements that is advantageous to the long-term strength of the concrete.

3.8 Series F: Varying the Aggregate/Cementitious Material Ratio

This series sought to make an additional investigation into the most effective aggregate/cementitious material ratio. A control group of the four mixes that had the highest 28-day compressive strengths from previous series were tested, as well as these same mixes with aggregate/cementitious material ratios of 0.8, 0.9, and 1.1. The mix designs of Series F are shown in Table 3.11.

Table 3.11 Series F Mix Design Proportions

	F1	F2	F3	F4	F5	F6	F7	F8
	D9	C15	D14	C17	D9, 0.9 sand	C15, 0.9 sand	D14, .9 sand	C17, .9 sand
Type III Cement	0	0.6	0.45	0.55	0	0.6	0.45	0.55
Silica Fume	0.1	0.125	0.125	0.05	0.1	0.125	0.125	0.05
VCAS ™	0	0.15	0.3	0	0	0.15	0.3	0
Fly Ash	0.2	0.125	0.125	0.1	0.2	0.125	0.125	0.1
Type I Cement	0.7	0	0	0.3	0.7	0	0	0.3
w/cm	0.2	0.201	0.201	0.201	0.2	0.201	0.201	0.201
agg/cm	1.00	1.00	1.00	1.00	0.90	0.90	0.90	0.90
HRWR (oz./cwt)	18.7	18.7	18.7	18.7	18.7	18.7	18.7	18.7

	F9	F10	F11	F12	F13	F14	F15	F16
	D9 .8 sand	C15, .8 sand	D14, .8 sand	C17, .8 sand	D9, 1.1 sand	C15 1.1 sand	D14, 1.1 sand	C17, 1.1 sand
Type III Cement	0	0.6	0.45	0.55	0	0.6	0.45	0.55
Silica Fume	0.1	0.125	0.125	0.05	0.1	0.125	0.125	0.05
VCAS ™	0	0.15	0.3	0	0	0.15	0.3	0
Fly Ash	0.2	0.125	0.125	0.1	0.2	0.125	0.125	0.1
Type I Cement	0.7	0	0	0.3	0.7	0	0	0.3
w/cm	0.2	0.201	0.201	0.201	0.2	0.201	0.201	0.201
agg/cm	0.80	0.80	0.80	0.80	1.10	1.10	1.10	1.10
HRWR (oz./cwt)	18.7	18.7	18.7	18.7	18.7	18.7	18.7	18.7

The behavior of the concrete varied significantly between aggregate/cementitious material ratios. The difference in behaviors is outlined in

Figures 3.23 and 3.24.

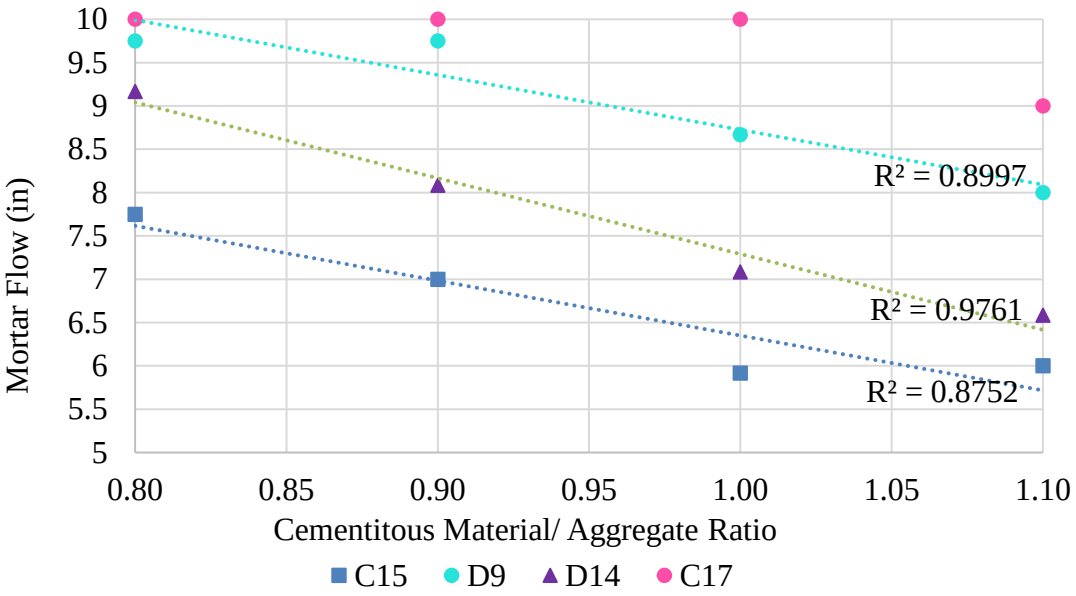

Figure 3.23 Aggregate/Cementitious Material Ratio vs. Mortar Flow

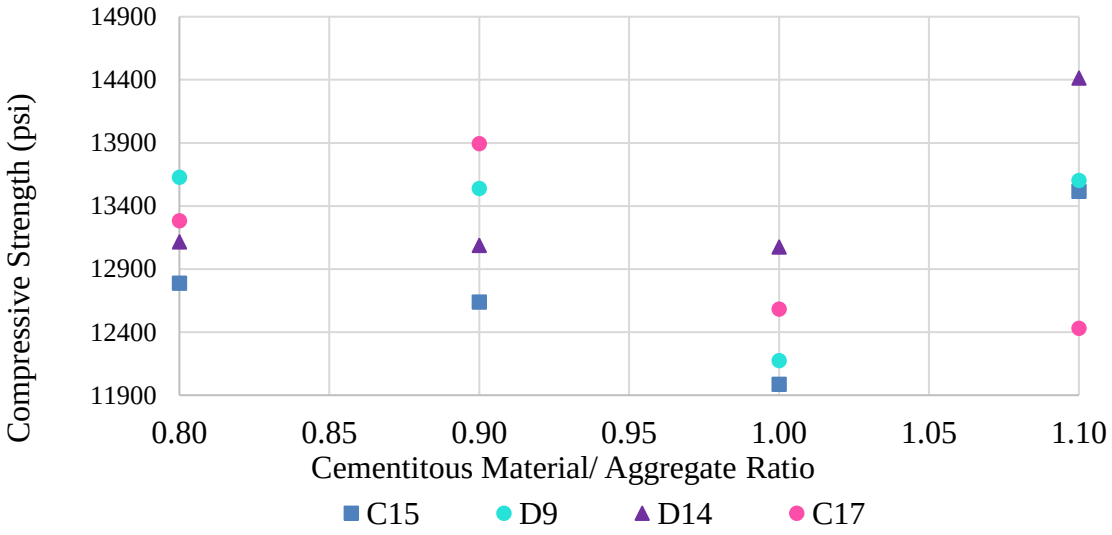

Figure 3.24 Aggregate/Cementitious Material Ratio vs. Compressive Strength

For all four mixes, there is a strong correlation between an increase in the aggregate/cementitious materials ratio and a decrease in mortar flow, as shown in Figure 3.23. Note that mix C17 exceeded the accurate capacity of the flow table for

some of these data points, so a correlation could not be determined. The compressive strength results shown in Figure 3.24, however, were not as conclusive.

A cursory look at the results in Figure 3.24 suggests that the aggregate/cementitious material ratio of 1.0 appears the weakest, and 1.1 the strongest. However, a comparison for each mix individually shows no general trend in aggregate/cementitious material ratio vs. compressive strength. There is no obvious reason to explain this phenomenon. As discussed earlier in the chapter for Series D, these aggregate/cementitious material ratios have significantly different particle packing potentials.

This series did not produce a clear correlation between the aggregate/cementitious material ratio and compressive strength. None of the strengths of this series exceeded those of previous series, even as the mixes were repeated exactly. The source of this discrepancy is unknown. However, these lower values were marked as the baseline the future series were compared against.

3.9 Series G: An Extensive Study into GGBFS

Because mixes in previous series had not yet achieved the target compressive strength, there was interest in investigating GGBFS as the primary SCM. Previous series had not investigated the effect of GGBFS without the addition of fly ash, and there was consideration that the two SCMs may not be as chemically compatible as other combinations of SCMs. Additionally, the literature indicated more success with GGBFS than previously found in this study though Series A-F (Kim et al., 2016). This discrepancy warranted further review of GGBFS. The mix designs for this series are given in Table 3.12.

Table 3.12 Series G Mix Design Proportions

	G1	G2	G3	G4	G5	G6	G7	G8
Type III Cement	0.85	0.75	0.65	0.55	0.8	0.7	0.6	0.5
Silica Fume	0.05	0.05	0.05	0.05	0.1	0.1	0.1	0.1
GGBFS	0.1	0.2	0.3	0.4	0.1	0.2	0.3	0.4
Type I Cement	0	0	0	0	0	0	0	0
w/cm	0.2	0.2	0.2	0.2	0.2	0.2	0.2	0.2
agg/cm	1.00	1.00	1.00	1.00	1.00	1.00	1.00	1.00
HRWR (oz./cwt)	18.7	18.7	18.7	18.7	18.7	18.7	18.7	18.7

	G9	G10	G11	G12	G13	G14	G15	G16
Type III Cement	0.75	0.65	0.55	0.45	0.7	0.6	0.5	0.4
Silica Fume	0.15	0.15	0.15	0.15	0.2	0.2	0.2	0.2
GGBFS	0.1	0.2	0.3	0.4	0.1	0.2	0.3	0.4
Type I Cement	0	0	0	0	0	0	0	0
w/cm	0.2	0.2	0.2	0.2	0.2	0.2	0.2	0.2
agg/cm	1.00	1.00	1.00	1.00	1.00	1.00	1.00	1.00
HRWR (oz./cwt)	18.7	18.7	18.7	18.7	18.7	18.7	18.7	18.7

	G17	G18	G19	G20	G21	G22	G23	G24
Type III Cement	0.75	0.65	0.55	0.45	0.65	0.55	0.45	0.35
Silica Fume	0.05	0.05	0.05	0.05	0.05	0.05	0.05	0.05
GGBFS	0.1	0.1	0.1	0.1	0.2	0.2	0.2	0.2
Type I Cement	0.1	0.2	0.3	0.4	0.1	0.2	0.3	0.4
w/cm	0.2	0.2	0.2	0.2	0.2	0.2	0.2	0.2
agg/cm	1.00	1.00	1.00	1.00	1.00	1.00	1.00	1.00
HRWR (oz./cwt)	18.7	18.7	18.7	18.7	18.7	18.7	18.7	18.7

	G25	G26	G27	G28	G29	G30	G31	G32
Type III Cement	0.5	0.4	0.3	0.2	0.4	0.3	0.2	0.1
Silica Fume	0.1	0.1	0.1	0.1	0.1	0.1	0.1	0.1
GGBFS	0.3	0.3	0.3	0.3	0.4	0.4	0.4	0.4
Type I Cement	0.1	0.2	0.3	0.4	0.1	0.2	0.3	0.4
w/cm	0.2	0.2	0.2	0.2	0.2	0.2	0.2	0.2
agg/cm	1.00	1.00	1.00	1.00	1.00	1.00	1.00	1.00
HRWR (oz./cwt)	18.7	18.7	18.7	18.7	18.7	18.7	18.7	18.7

Given the previous series, it was anticipated that increased silica fume would decrease mortar flow, and increasing Type I cement would increase mortar flow.

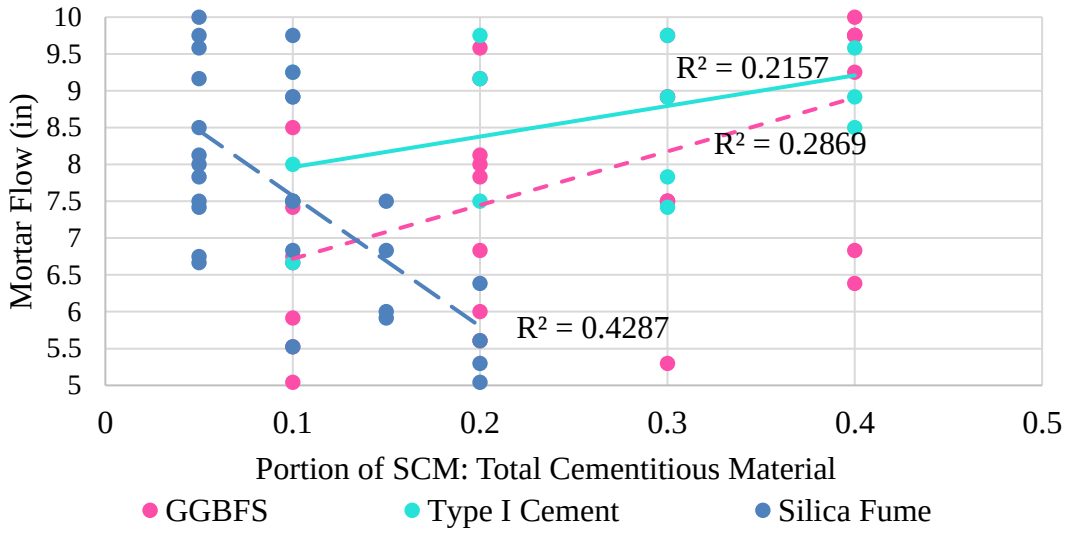

Figure 3.25 SCM and Type I Cement vs. Mortar Flow

However, the results shown in Figure 3.25 indicate that there is not a compelling correlation between silica fume, GGBFS, or Type I cement and mortar flow. High levels of silica fume proved to reduce mortar flow in Series D and high levels of Type I cement proved to increase mortar flow in Series E, but the results in Figure 3.25 would indicate the interaction between these constituents is also influential. The mixes with less than 6.5 in. mortar flow were tamped in the manner according to ASTM C109.

These combinations, with the same amount of HRWR and water as previous mixes, varied significantly in texture from previous mixes. This difference in texture is not directly measurable in the mortar flow. The fly ash mixes had a very sticky consistency; it would trail down the front of the cup used to pour the concrete into the mold, stick to the sides of the mixing bowl, and leave a trail on the mortar flow table. In contrast, the GGBFS mixes were very cohesive. Whether a greater than 10 in. mortar

flow or less than 5 in. mortar flow, the GGBFS mixes did not stick to the side of the bowl, and never stuck to the pouring side of the cup.

This cohesiveness made low mortar flow GGBFS mixes difficult to tamp if the rubber tamper was not completely clean. After repeated tamping, the mix would coat the rubber tamper. When a coated tamper went into the mix, it would pull up the entire mass that had been placed in the mortar cube. This led to specimens having holes and gaps in corners that could not be effectively tamped out. This issue may have led to artificially low compressive strengths for these low-mortar flow GGBFS mixes.

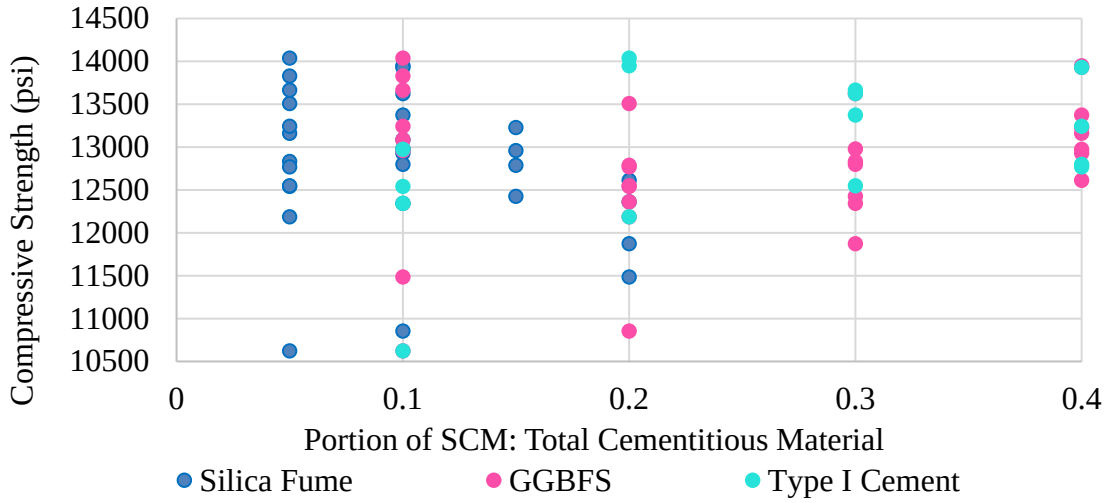

Figure 3.26 SCM and Type I Cement vs. 28-Day Compressive Strength

The general trends seen in the mortar flow were repeated in the compressive strength data shown in Figure 3.26. Silica fume generally weakened the concrete as replacements rates increased, whereas GGBFS and Type I cement both resulted in compressive strength improvements with larger replacements. However, the GGBFS and Type I cement replacements had more modest impacts than that of the silica fume. A display of compressive strengths by mix is shown in Figure 3.27.

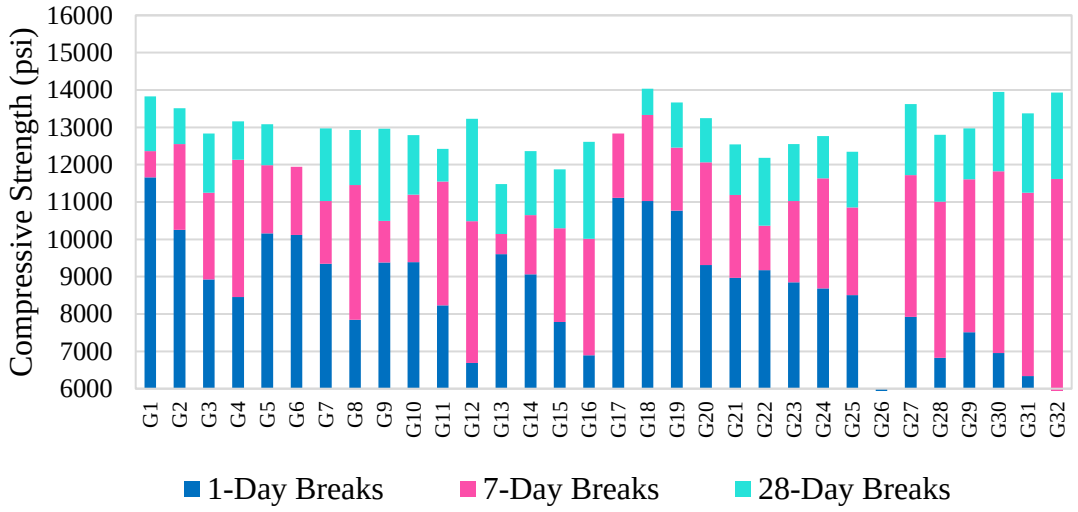

Figure 3.27 Compressive Strengths of Series G

There were three mixes in this series, G18, G30, G32, that had comparable compressive strengths to those of Series F. Though direct correlations between individual SCMs and cements were inconclusive, these mixes demonstrated some similarities to the strongest mixes. These mixes demonstrated that high levels of GGBFS and Type I cement interacted advantageously with low replacements of silica fume. While the three best mixes of this series were not directly repeated in future iterations, the commonalities of the best mixes were used to build very successful mixes in Series J.

3.10 Series H: Reviewing the Literature

A paper was published by Ibrahim during the course of this research that reported a set of mix designs that produced UHPC using typically available materials. The mixes of Series H were notably different from the mixes developed through Series A-G with their increase in HRWR and very significant increase in the aggregate/cementitious material ratio. The amount of sand was increased. Ground silica

was also added as a filler, instead of exclusively using unhydrated cementitious materials to fill the particle gaps.

These mixes were attempted, with two additional investigative iterations. The mix designs of Series H based on this research are shown in Table 3.13.

Table 3.13 Series H Mix Design Proportions

		H1	H2	H3	H4	H5	H6	H7	H8	H9
Silica Fume		0.10	0.10	0.10	0.10	0.10	0.10	0.10	0.10	0.10
VCAS		0.00	0.00	0.00	0.00	0.00	0.00	0.00	0.00	0.00
Fly Ash		0.09	0.09	0.09	0.09	0.09	0.00	0.00	0.00	0.09
GGBFS		0.00	0.00	0.00	0.00	0.00	0.09	0.09	0.09	0.00
Type I Cement		0.81	0.81	0.81	0.81	0.81	0.81	0.81	0.81	0.81
agg/cm		1.16	1.42	1.42	1.42	1.42	1.42	1.42	1.42	1.42
Silica/ agg	**10 Micrometers**		0.11	0.18				0.11		
	15 Micrometers				0.11	0.18			0.11	
w/cm		0.20	0.20	0.20	0.20	0.20	0.20	0.20	0.20	0.20
HRWR (oz./cwt)		22.7	20.2	20.2	20.2	20.2	20.2	20.2	20.2	20.2

The compressive strengths of Series H are shown in Figure 3.28.

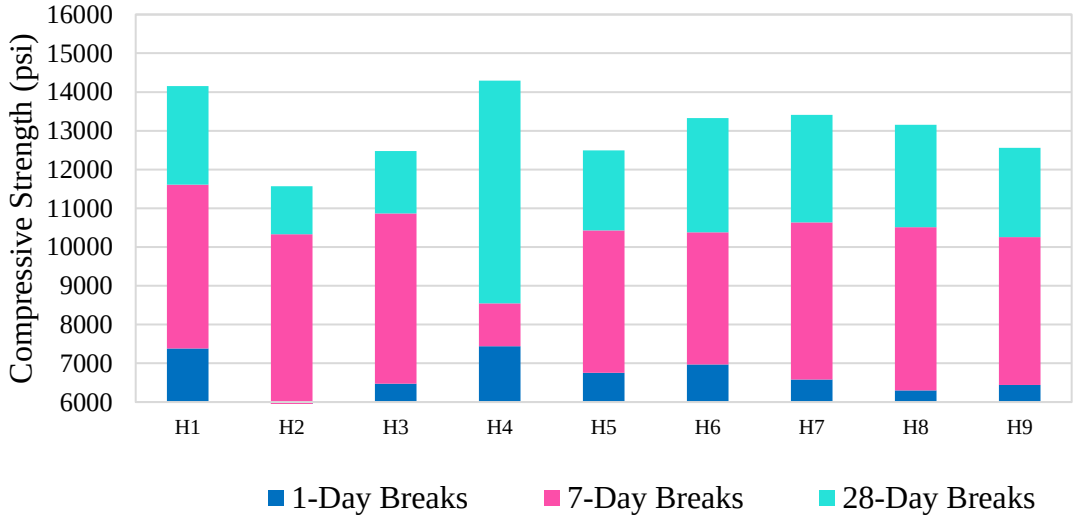

Figure 3.28 Compressive Strengths of Series H

The strengths displayed in Figure 3.28 of Series H were comparable, though weaker, to those of previous series. The two strongest mixes of the series, H1 and H4, required an additional and expensive constituent, ground silica. Given these mixes were not as strong but were more expensive, these mixes were not used in further iterations.

3.11 Series J: Combining Promising Variables

The mixes of Series J sought to investigate a variety of small changes in successful mixes from the previous series. Intended to be the last set of mixes before moving into large-scale testing, this series was a catch-all for a variety of small changes that could cause improvements in compressive strength. The first set of mixes, J1 through J4, investigate GGBFS replacements with only Type I and no Type III cement. This is a continuation of promising combinations of cements and SCMs from Series G. The second set of mixes, J5 through J6, investigate the use of a different HRWR. The third set of mixes, J7 through J9, replace the Type III cement in the best performing mixes with Type I cement. The final set of mixes, J10 through J13, explore the aggregate/cementitious material ratios that appeared promising in Series F. These mix designs are displayed in Table 3.14.

Table 3.14 Series J Mix Design Proportions

	J1	J2	J3	J4	J5	J6	J7
Type III Cement	0	0	0	0	0.55	0.55	0
Silica Fume	0.1	0.1	0.1	0.1	0.05	0.05	0.125
VCAS ™	0	0	0	0	0	0	0.15
Fly Ash	0	0	0	0	0.1	0.1	.125
GGBFS	0.1	0.2	0.3	0.4	0	0	0
Type I Cement	0.8	0.7	0.6	0.5	0.3	0.3	0.6
w/cm	0.2	0.2	0.2	0.2	0.2	0.2	0.2
agg/cm	1.00	1.00	1.00	1.00	1.00	1.00	1.00
HRWR (oz./cwt)	18.7	18.7	18.7	18.7	23	23	18.7

	J8	J9	J10	J11	J12	J13
Type III Cement	0	0	0.3	0.1	0.3	0.1
Silica Fume	0.1	0.05	0.1	0.1	0.1	0.1
VCAS ™	0.15	0	0	0	0	0
Fly Ash	0.15	0.1	0	0	0	0
GGBFS	0	0	0.2	0.4	0.2	0.4
Type I Cement	0.6	0.85	0.4	0.4	0.4	0.4
w/cm	0.2	0.2	0.2	0.2	0.2	0.2
agg/cm	1.00	1.00	1.00	1.00	1.00	1.00
HRWR (oz./cwt)	18.7	18.7	18.7	18.7	18.7	18.7

This series displayed some of the highest compressive strengths in the experiment. However, the GGBFS mixes with the highest strengths (J3, J4) had very low early strengths because they lack Type III cement. While the final strength of the concrete was the primary design criteria, one of the anticipated benefits of UHPC is that high early strengths return vehicular traffic to the bridge as soon as possible. Low early strength performance was not disqualifying for these mixes, however, as the effect of heat curing on early strength gain had yet to be investigated. Additionally, many of these high-strength mixes had very high mortar flows, which had to be considered as a benefit (easier to mold) and detriment (may not suspend fibers). These strengths are displayed Figure 3.29.

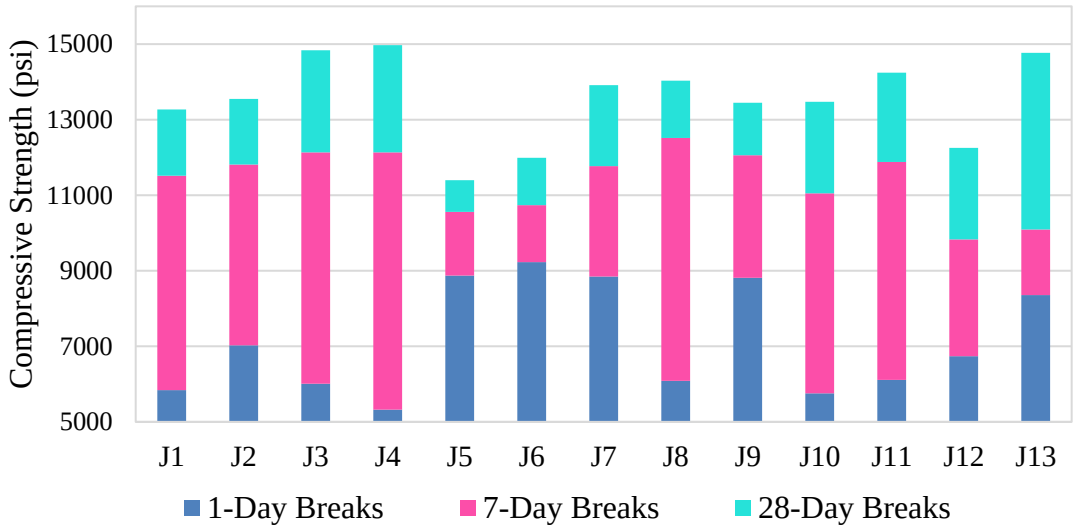

Figure 3.29 Compressive Strengths of Series J

Three of the mixes in the series were the strongest in the experiment since Series F. The three of the strongest mixes feature the combination of high levels of GGBFS and Type I cement and low levels of silica fume that showed promise in Series G. The mixes with fly ash and VCAS™ had increased 28-day compressive strength using only Type I cement and no Type III cement. None of these mixes, J5-J9, had strengths as high as the GGBFS mixes. However, a mix without GGBFS as the primary SCM was desired for the next stage of testing, as might show advantages in other properties.

3.12 Mix Design Development Study Summary

There are several key takeaways from this study. It was established that the constituents available in Oklahoma were unlike those available to Graybeal or Ibrahim, as their mixes did not yield the reported results. It was also established that the chemical reactions and compatibility was as important as physical compatibility, as particle packing did not directly result in higher compressive strengths.

There were also more specific lessons gleaned from this study. The optimal w/cm ratio was found to be 0.2. The strongest mixes have 40-50% cumulative SCM replacement, 10-12.5% of that being silica fume. Using high proportions of Type I to Type III cement produced the strongest mixes, and many of the strongest mixes have no Type III cement. The GGBFS worked well in higher replacements, 30-40%, with silica fume and Type I. The strongest fly ash mixes had equal amounts of VCAS ™, typically in the 12.5-15% replacement range. The mix designs, as well as the mortar flow and the compressive strength data is provided in full in Appendix A.

The mixes with the highest compressive strengths stood out as candidates for the next phase of testing. These mixes are listed below in Table 3.15, as well as their benefits and detriments.

Table 3.15 Final Mix Candidate Benefits and Detriments

		J3	J4	J8	J13
Mortar Flow (in)		10.25 estimated	15 estimated	13 estimated	10
Compressive Strength (psi)	1-Day	6010	5330	6080	8360
	7-Day	12130	12140	12520	10090
	28-Day	14840	14970	14030	14770
Benefits:		Very workable texture and mortar flow	Strongest mix tested	Best FA mix, sticky texture likely to suspend fibers well	Best early strength, mortar flow likely to suspend fibers
Detriments:		Low early strength	Research notes say "flows like water" - not likely to suspend fibers. Very low early strength	Low early strength	

4 Heat Curing and Fiber-Reinforcement Study

4.1 Introduction

The goal of this section's research was to integrate steel fibers and investigate the benefits of heat curing. Steel fibers are used as the exclusive tensile reinforcement in UHPC, and experiments had to be conducted to ensure the fibers would remain evenly dispersed. Heat curing was investigated in an attempt to increase the early strength of the concrete. This study hoped to discern the time required to reach the full heat curing potential, as well as determine the differences in efficacy between mixes. These are the last investigations into the mix design before the mixes' properties will be analyzed. For the purpose of this portion of the research, Mixes J8, J3, and J13 were relabeled as Mixes A, B, and C, respectively.

4.2 Optimizing Mortar Flow

The first attempt at a large mix resulted in some unforeseen issues. The transition from the 0.1 ft^3 mixes in the Blakeslee planetary mixer to a 1.3 ft^3 mix in the Mortarman paddle mixer resulted in additional mortar flow, as well as leaving unhydrated lumps of cementitious material. The mortar flow of the first mix was approximately 12 in. and was theoretically in the acceptable range. However, the fibers segregated in this mix immediately after being added. It was clear that the mortar flow would have to be reduced in order to suspend the fibers in future mixes.

To address this problem, this mix was reformulated with half the HRWR, and 5 mL was added at a time to monitor the effect on the texture and mortar flow. As part of this process, one 3 in. x 6 in. cylinder's worth of concrete was removed from the batch,

and fibers were added. This step was repeated with additional HRWR added in 5 mL increments until the fibers visibly settled. The mortar flow at the "settling point" was found to be 8.75 in. for Mixes B and C, the two GGBFS mixes, and 8.25 in. for Mix A, the fly ash and VCAS™ mix. The target flow of 7.75 in. was selected for Mix A and 7.0 in. was selected for Mixes B and C, anticipating an additional 0.5 in. of mortar flow from the small to big mixture translation. These targets produce a 2-in. tolerance of mortar flow, given that a 6-in. mortar flow is necessary to "break" a mix and the fibers will begin to segregate at a mortar flow of 8.25 in.

The three mixes were repeated until the amount of HRWR caused the desired flow without having to add any additional HRWR after the standard mixing regime. Earlier mixes indicated that HRWR added after the mix had broken was not as effective as the HRWR that was added in the method described in Chapter 3. The mixes were re-designated for clarity, in progressive order of compressive strength. The final mix designs used are presented below in Table 4.1.

Table 4.1 Mixes with Final Proportions of HRWR

	A (J8)	**B (J3)**	**C (J13)**
Type III Cement	0.00	0.00	0.10
Silica Fume	0.10	0.10	0.10
VCAS™	0.15	0.00	0.00
Fly Ash	0.15	0.00	0.00
GGBFS	0.00	0.30	0.40
Type I Cement	0.60	0.60	0.40
w/cm	0.20	0.20	0.20
agg/cm	1.00	1.00	1.00
HRWR (oz./ cwt)	15.77	15.77	14.88
Mortar Flow (in.)	7.00	7.75	7.75

These mix designs required a reduced dosage of HRWR compared to previous iterations. Mixes A and B required the same amount of HRWR, though they resulted in different textures. Mix C required a further reduction in HRWR. The reduction of the HRWR did not require longer mixing time in the small mixer, but it was anticipated that the large mixer might require additional time for the mix to "break" and to break up the clumps of cementitious material.

4.3 Effects of Heat Curing and Fiber Reinforcement

To study the effects of heat curing and fiber reinforcement, two sets of experiments were conducted. The first set of mixes established the efficacy of heat curing and the fibers as independent variables. The second set of mixes studied the combination of fiber reinforcement and heat curing. To ensure that the differences in heat cured and fiber reinforced specimens would be independent of batching errors, large batches were mixed in the Mortarman mixer and multiple factors tested. The specimens were changed from mortar cubes to 3 in. x 6 in. cylinders to accommodate the fibers. The specimens were demolded at 12 hours and were moist cured. Before testing, the ends of the cylinders were ground smooth with a machine to ensure a consistent breaking surface, according to ASTM C39. Given the high strengths of these mixes, the loading rate of the cylinders was increased to 150 psi/s, which is standard for testing UHPC mixes.

In addition to readjusting the dosage of HRWR, adjustments from the previous mixing method had to be made to accommodate the large mixer and different specimen size. The dry constituents were not broken up as effectively by the Mortarman as the planetary mixer, as there was no high speed to add shear and break up the large

particles. Clumps in the dry constituents had to be broken down manually before water was added. The last stage of mixing took 5 minutes in the Mortarman, given there was no “speed 2” to add shear in the larger mixer.

4.3.1 Fiber Reinforcement

Fiber reinforcement serves to replace traditional steel reinforcement in UHPC, and like traditional reinforcement, primarily serves to increase the tensile performance. The fibers are not intended to significantly increase the compressive strength, though there should be a small bump as the fibers produce some confinement in the concrete. Fibers were added at a rate of 2% by volume, the upper bound of the most effective replacement according to Graybeal (2013).

Each of the mixes in the study required both concrete with and without fibers. The portion needing fibers was removed, and the appropriate amount of fibers was mixed in by hand before casting, as seen in the photographs in Figure 4.1 and Figure 4.2.

Figure 4.1 Fibers Batched

Figure 4.2 Hand-Mixing Fibers

Two types of fiber reinforcement were tested. Both fibers were crimped, with dimensions of 0.18 in. x 0.033 in. x 1 in. The fibers tested were carbon steel and Grade 430 stainless steel. The effect of these fibers on the compressive strength is shown in Figure 4.3.

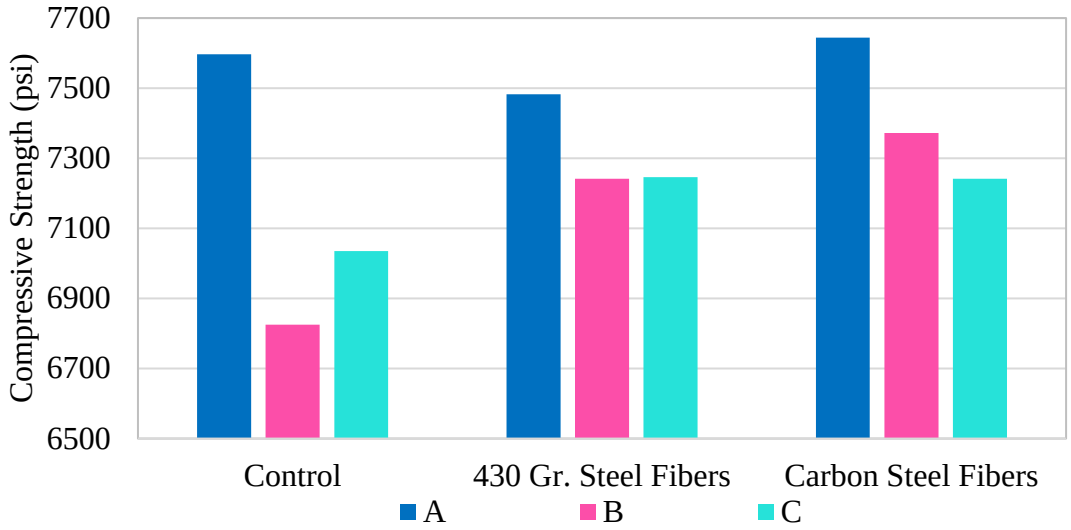

Figure 4.3 Fiber-Reinforced Compressive Strength at 1 Day

These mixes do not show a significant strength increase due to the fibers or difference between the fibers at 1 day. Figure 4.4 shows that this conclusion holds for the compressive strength at 28 days. The specimens with fibers had less variation between specimens than the control.

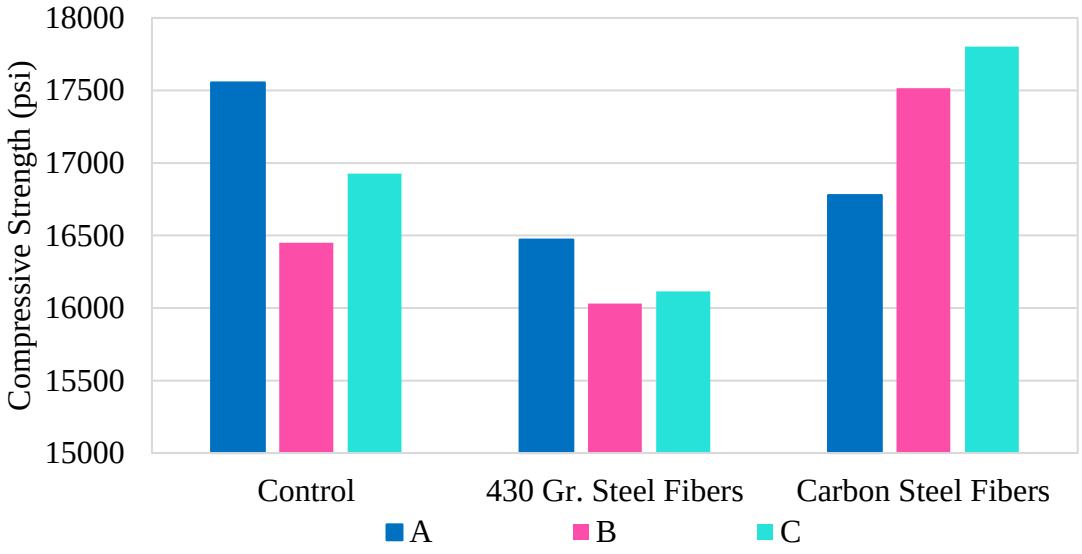

Figure 4.4 Fiber-Reinforced Compressive Strength at 28 Days

While there is not a significant difference in compressive strengths, there is a large difference in the behavior at failure between the reinforced and unreinforced specimens, as shown in Figure 4.5 and Figure 4.6. The fiber reinforced specimens retain some continuity of shape upon failure whereas the non-fiber-reinforced specimens shattered.

Figure 4.5 Unreinforced Cylinder After Breaking

Figure 4.6 Reinforced Cylinder After Breaking

The fibers appear to make a small (0% to 6%) contribution to the compressive strength at 1 day, but the lack of correlation between any individual mix or type of fiber suggests there is not a strong relationship. The same lack of consistency in the data at 28 days suggests there is no long-term compressive strength benefit. However, the fibers did prevent failures from exploding by producing confinement.

4.3.2 Heat Curing

The application of heat serves to accelerate concrete curing. UHPC applications, including bridge joints, often require quick turnaround from casting to service. The target for this turnaround is typically 3 days, so the heat cured specimens in this study were tested at this time frame. A related experiment conducted on UHPC joints indicated that the highest temperature held consistently at the center of the joint was

180°F (82°C), so this was selected as the oven temperature, ensuring this experiment would be field applicable.

While field joints would have applied heat immediately after the concrete had been poured, the laboratory required a slightly different curing method. The cylindrical specimens were kept covered until they could be demolded at 12 hours, when they were labeled and placed in the oven. To maintain high moisture in the oven, specimens were placed in tins which were filled ¾ full of water, and sealed in an oven bag. This setup is seen in Figure 4.7 and Figure 4.8. Specimens were removed from the oven after 12, 36, and 48 hours of heat curing. The specimens were allowed to come to room temperature for 2 hours before being placed in curing tubs kept at 68°F (20°C). The specimens were tested at the same time, at 3 days.

Figure 4.7 Cylinders in Oven Bag

Figure 4.8 Specimens Heat Curing

Heat curing made a considerable impact on the compressive strength of these specimens, as seen in Figure 4.9.

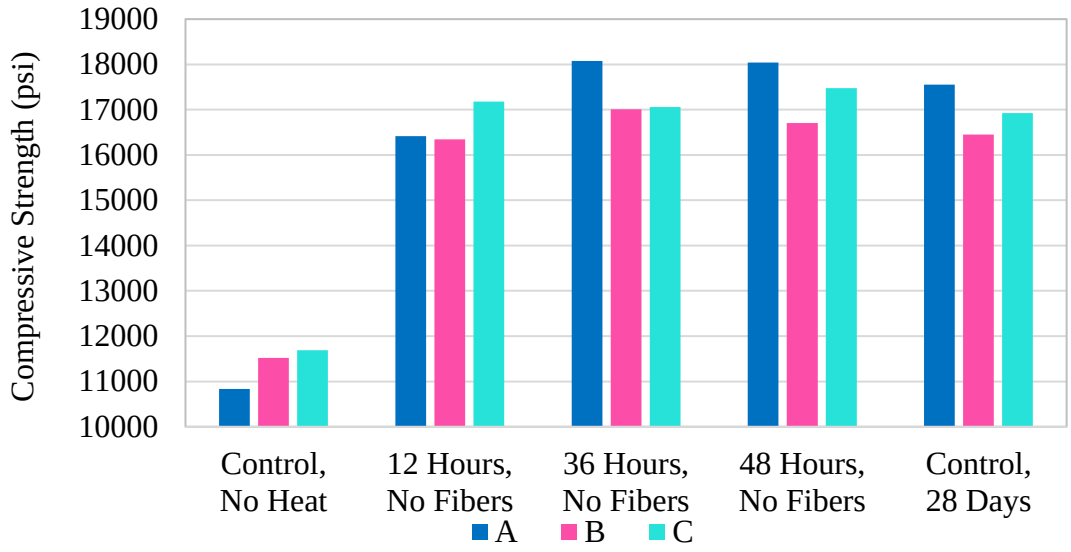

Figure 4.9 Compressive Strength at 3 Days, Heat Cured

The results for heat curing of the UHPC specimens is shown in Figure 4.9. There is nearly 50% improvement across each mix between the control and 12 hours of heat curing. The improvement between 12 hours, 36 hours, and 48 hours is not as dramatic, especially for the mixes where GGBFS is the primary SCM, Mixes B and C. There are only small differences between heat curing 12 and 48 hours for these mixes, and are not compellingly correlated. Both of these mixes had met or exceeded 28-day strengths after 12 hours of heat curing. The mix in which VCAS and fly ash were the primary SCMs, Mix A, saw a marked improvement between 12 and 36 hours. This mix took 36 hours of heat curing to exceed the compressive strength at 28 days. There was no discernable difference in the way the specimens failed.

4.3.3 Heat Curing and Fiber Reinforcement

Given that the fiber-reinforced UHPC will be heat cured in the field, the combined effect of these elements must be studied. Fiber reinforcement is reported to work beneficially with heat curing, as the fibers promote more even heat dispersal. To

reduce variables, only Gr. 420 steel fibers were used in this experiment. Figure 4.10 compares the effects of heat curing with and without fibers.

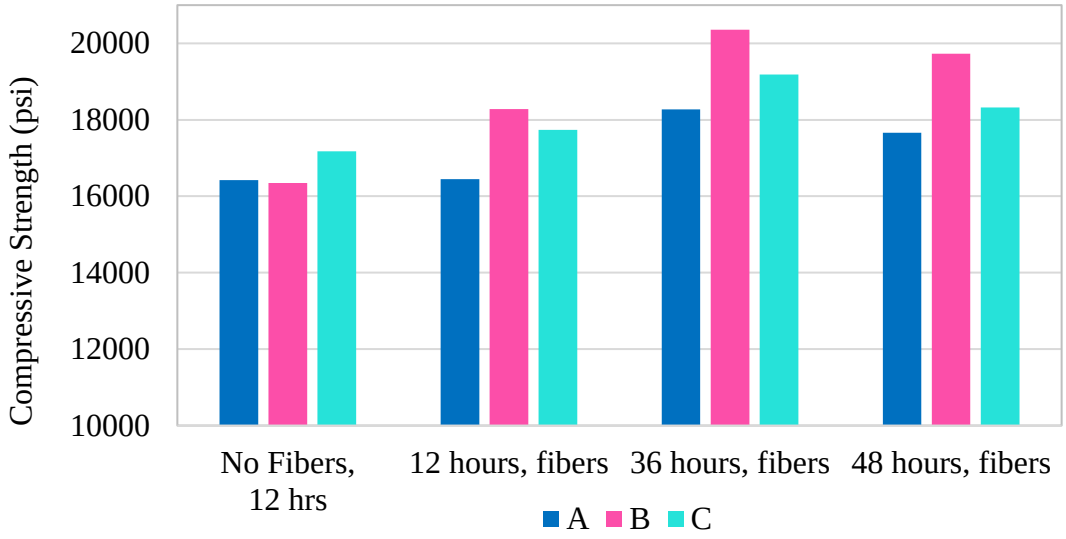

Figure 4.10 Compressive Strength at 3 Days, Fiber-Reinforced and Heat Cured

The combination of fibers and heat curing led to marginal improvements in the compressive strength, as seen in Figure 4.10. Like the heat-cured specimens without fibers, Mix A required longer exposure to heat to make the gains in strength seen in Mix B and Mix C. Every mix exceeded the compressive strength without fibers after 36 hours. The specimens cured for 48 hours were weaker than the specimens cured for 36 hours. The reason for this phenomenon is unknown. It is unclear if the confinement effect of the fibers caused the increase in strength gain over the control, or if the fibers allowed the heat to penetrate more quickly and increase the effectiveness of the heat curing. This observation is further explored in Figure 4.11.

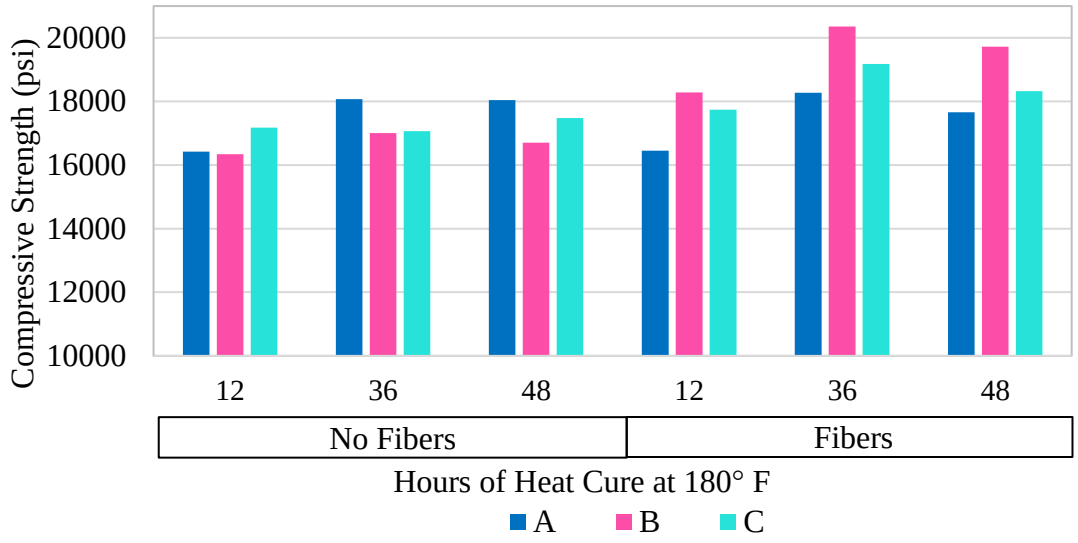

Figure 4.11 Compressive Strength at 3 Days, Heat Cured, Unreinforced and Fiber-Reinforced Specimens

As shown in Figure 4.11, the fiber reinforced specimens outperformed the unreinforced specimens at all comparable heat curing levels, though by small increments (except fiber reinforced Mix A at 36 hours, which specimens had anomalously low compressive strengths). As noted earlier, there was a more significant difference between the fiber reinforced and non-fiber-reinforced specimens at 36 and 48 hours than at 12 hours.

4.4 Heat Curing and Fiber-Reinforcement Study Summary

Altogether, the combination of heat curing and fiber reinforcement was more beneficial than either factor independently. Heat curing at 180°F for an excess of 12 hours increased the acceleration of curing such that the compressive strength at 3 days exceeded the compressive strength at 28 days. A majority of the strength gain occurs in the first 12 hours of heat curing, though there are additional gains at 36 hours. In this experiment, there were no gains observed from 36 to 48 hours. The fiber reinforcement

did not pose significant advantages in compressive strength, but did prevent explosive failures. Ultimately, the gains with the combination of fiber-reinforcement and 36 hours of heat curing resulted in a mix exceeding 20 ksi at 3 days.

5 Heat Curing and Fiber-Reinforcement Study

5.1 Introduction

This section reports the results of non-compressive material property testing of the three mixes, A, B and C, that were chosen in Chapter 4. The MOR (modulus of rupture) was tested both with and without fibers in order to compare the efficacy of the reinforcement fibers in tension. Additionally, MOE (modulus of elasticity) and abrasion tests were conducted on the concrete without fibers. These tests were conducted to further define the behavior of UHPC, given that compressive strength has been the only property studied in the development of these mixes.

5.2 MOE Testing

The modulus of elasticity reflects the ability of a material to deform elastically. The modulus of elasticity was calculated for each mix according to a modified ASTM C469. The cylinders were loaded at a rate of 150 psi/s, to be consistent with the procedure in the rest of the study. The MOE testing apparatus is shown in Figure 5.1.

Figure 5.1 MOE Test Setup

UHPC mixes typically have MOEs in the range of 6,000-10,000 ksi, and mixes with similar strengths and curing conditions to mixes A, B, and C, have MOEs close to 6,200 ksi (Graybeal, 2006; Russel and Graybeal, 2013).

The moduli of elasticity for mixes A, B and C derived experimentally were compared to the conventional equation relating compressive strength to modulus of elasticity cited in the ACI 318 building code (2014), shown in Equation 5.1.

$$E_c = 57{,}000\sqrt{f'_c} \qquad \text{(Eq. 5.1)}$$

This equation relates modulus of elasticity, E_c (psi), to the square root of the concrete compressive strength, f'_c (psi).

Because Equation 5.1 is known to overestimate the MOE of high strength concretes, Russel and Graybeal proposed a modified equation, Equation 5.2, for f'_c (psi) values between 4,000 and 28,000 psi, in the same terms (2013).

$$E_c = 46{,}200\sqrt{f'_c} \qquad \text{(Eq. 5.2)}$$

The MOE of each mix, shown in Figure 5.2, was experimentally determined and compared to the anticipated performance of Equations 5.1 and 5.2

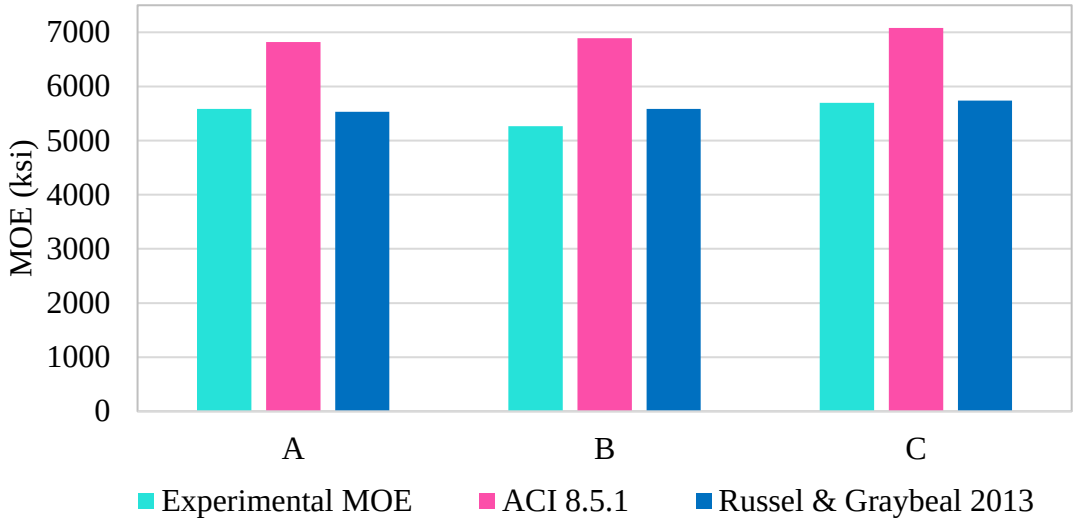

Figure 5.2 Modulus of Elasticity

Mixes A and C have similar MOEs, greater than 5,500 ksi. Mix B has a MOE about 7% lower, at about 5,300 ksi. Given that mixes B and C are more similar in composition, a correlation between specific constituents and MOE is unlikely. More specimens would be required to determine if the difference between these mixes are significant. The ACI 318-14 model produces a consistent overestimation of 20%. The model proposed by Russel and Graybeal, however, only differs from the actual values by 1%, which is excellent.

Mix B has a MOE slightly lower than the other two mixes, though all have a MOE around 5,500 ksi. The typical ACI equation overestimates the MOE. This was expected, as the equation is known to be less accurate, the higher the compressive strength of the concrete. The equation proposed by Russel and Graybeal was very accurate, however, and could be confidently used in design.

5.3 Abrasion Testing

Abrasion tests serve to compare the resistance to wear of one sample to another. The standard of comparison for this study is Ductal®, a commercially available UHPC product. The abrasion tests in this study were conducted according to ASTM C944, slightly modified. UHPC has been noted to be resistant to abrasion, so the double-load of 44 pounds was applied normal to the testing surface (Graybeal, 2006). Additionally, the rotating cutter was spun at 230 rev/min to accommodate the Type KSD- 42H universal drilling machine that was available. The abrasion test setup is shown in Figure 5.3.

Figure 5.3 Abrasion Testing Setup

Casting UHPC in-place typically results in a wood formwork casting surface, a troweled surface, or a ground surface. The baseline of comparison for this study, Ductal®, is typically cast in place 0.25 in. over grade, and ground off to grade. Because broken specimens of mixes A, B, and C indicate that the bubbles in these mixes are evenly distributed, it was deemed unlikely that there is an advantage to grinding the surface of the mixes developed in this study. Because grinding is the most expensive

option and it has not been determined necessary, the two surfaces of interest in this study are wood-cast surfaces and troweled surfaces. The wood-cast surface is a better evaluation of the abrasion resistance of the concrete, and the troweled surface is a better evaluation of how the roughness of the finished surface of each mix effects the abrasion resistance. The results of the abrasion resistance tests are shown in Figure 5.4.

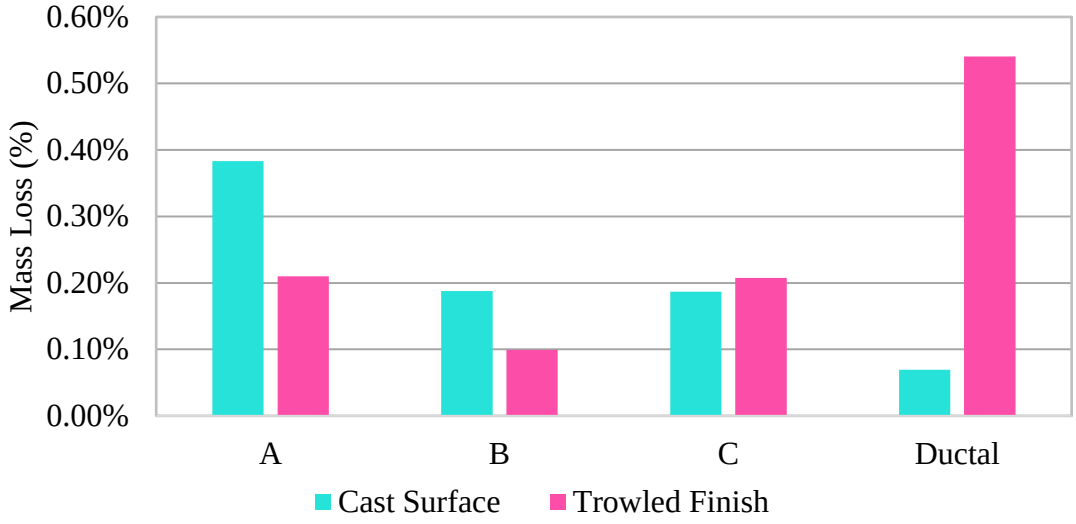

Figure 5.4 Abrasion Resistance

The cast surface concrete provides a consistent comparison of the properties of the concrete. Mix A, with fly ash and VCAS™, has nearly half the abrasion resistance than the Mixes B and C, with GGBFS. The cast surface of Ductal® has nearly twice the abrasion resistance of the mixes formulated in this study.

The troweled surface provides a comparison of the surface texture of the specimens, and how that surface affects the abrasion resistance. In this study, Ductal® had less abrasion resistance than the formulated mixes. The three formulated mixes had similar visual surface characteristics, and similar abrasion resistances compared to the Ductal®. Mix B had less visual bubbles after abrasion, and had nearly twice the

abrasion resistance as the other formulated mixes. To explain how the troweled surface is different from the cast surface, the surface textures were investigated.

Typical concrete would provide a consistent finish with a trowel, but the UHPC behaves differently. Trowels are only necessary with UHPC to screed off excess concrete, given the paste will flow and make an even, smooth surface. However, bubbles continue to rise to the surface, even after the bench taps used for consolidation. The mixes formulated in this research, A, B, an C, had smooth surfaces that were slightly lumpy. The Ductal®, however, had a rough, bubbly surface. This difference in surface texture between the Ductal® and Mix C, which is representative of the formulated mixes, had a considerable impact on the abrasion resistance, as shown in Figures 5.5 and 5.6.

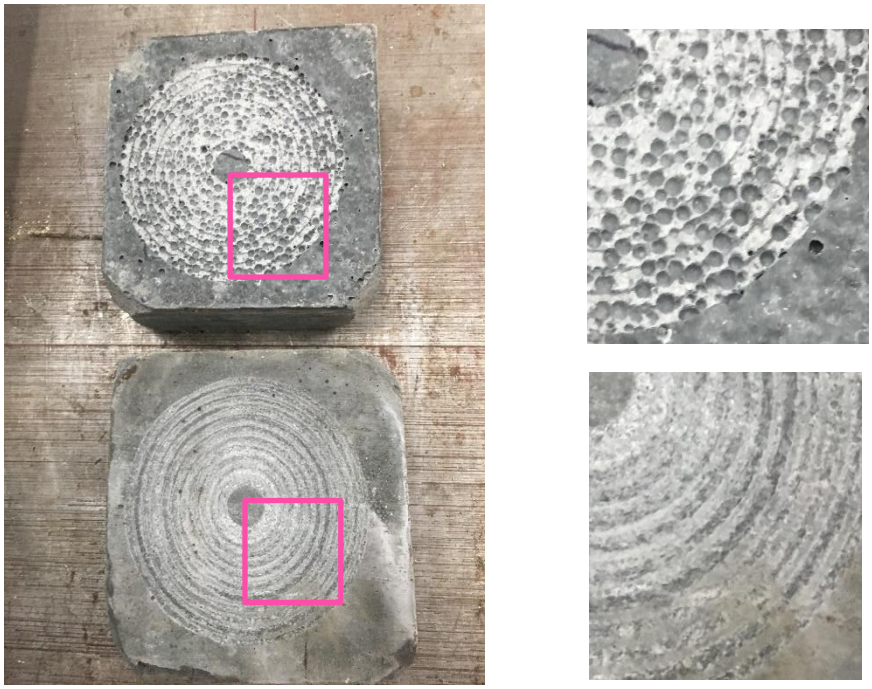

Figure 5.5 Abraded Ductal® Specimens
(Troweled Surface Above, Cast Surface Below)

Figure 5.6 Abraded Mix C Specimens
(Troweled Surface Above, Cast Surface Below)

Visual inspection shows that the Ductal® surface has more post-consolidation bubbles than Mix C, and that this led to increased abrasion as the bubbles provided more surface area to abrade. However, the bubbles on the surficial crust of the Ductal® would be ground off, and the surface exposed would be the interior of the sample, so this surface is not representative of how the material would be used in the field.

While the bubble warts occur less frequently on the formulated mixes, these mixes also show a discolored surficial crust that may indicate different properties, including abrasion resistance. This discoloration is shown in Figure 5.7.

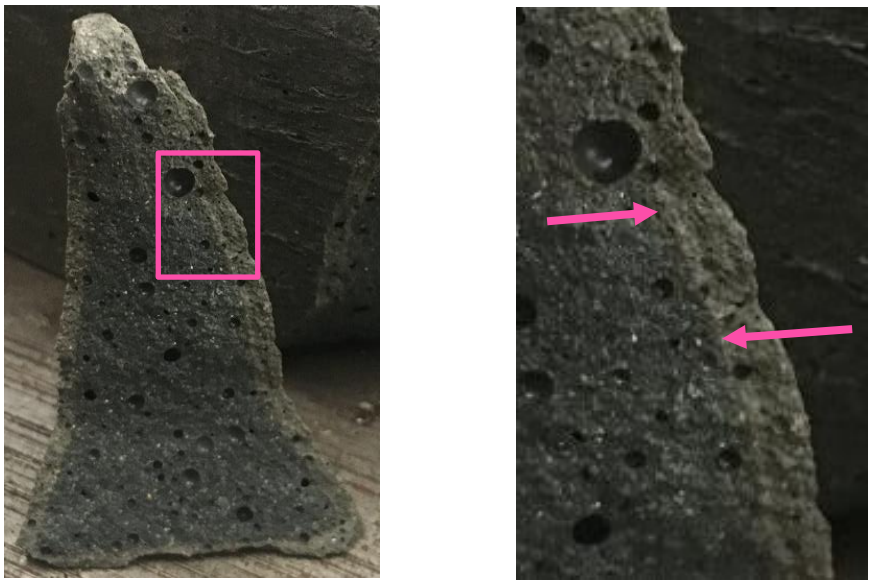

Figure 5.7 Mix C Surficial Crust Discoloration

This study concluded that Ductal® had superior abrasion properties compared to the formulated mixes. However, while Ductal® requires grinding off the surface, the formulated mixes may not require this expensive extra step, given the bubbles are evenly dispersed and the natural surface may have sufficient abrasion resistance. Additional study comparing the abrasion resistance of UHPC vs. typical pavement and

non-proprietary UHPC vs. Ductal® is necessary to determine the comparative abrasion resistance of non-proprietary UHPC.

5.4 MOR Testing

The modulus of rupture reflects the ultimate stress of a concrete member in bending. Because concrete is much weaker in tension than compression, failure in flexure reflects the tensile strength. The MOR of the unreinforced concrete was determined according to ASTM C78, and the first-cracking MOR of the fiber-reinforced concrete was determined according to ASTM C1609, slightly modified.

The unreinforced specimens were downsized to 3 in. x 3 in. x 11 in., and loaded at the maximum allowable rate, 175 psi/min. The fiber-reinforced specimens were cast at the size recommended for mixes with fibers 1 in. long, 4 in x 4 in. x 14 in. In absence of the machinery required to enforce a constant deformation, a loading rate of 175 psi/min was applied. Both tests followed the setup in Figure 5.8.

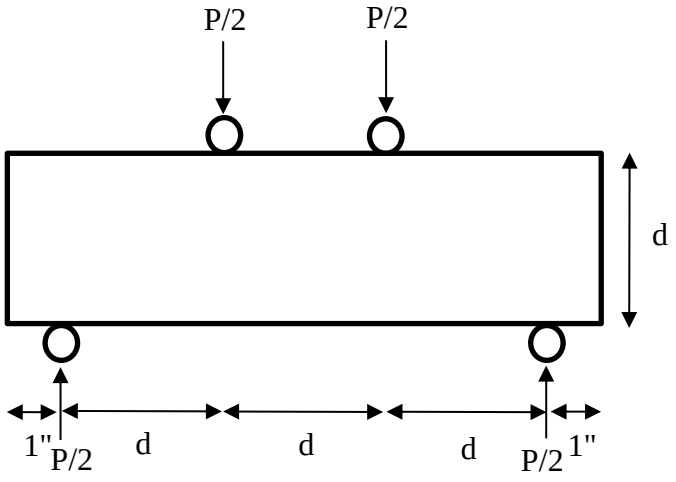

Figure 5.8: MOR Testing Configuration

MOR testing with unreinforced UHPC is uncommon. Most MOR tests conducted assume fiber reinforcement, in order to characterize how UHPC would be used in the field. However, given the MOR of the unreinforced specimens will be the strength at the first crack, the results of the tests were anticipated to be similar in magnitude. Typical first-cracking strength for fiber-reinforced concrete is reported between 0.98 to 2.00 ksi (Aghdasi et al., 2016). Mixes with the typical steel fibers at 2% replacement are expected to perform at about 1.11 ksi, based on similar research (Aghdasi, et al., 2016). Russel and Graybeal found the first-cracking tensile strength to be 1.3 ksi for untreated specimens with a compressive strength of 18 ksi (2013). The results of these tests are shown in Figure 5.9.

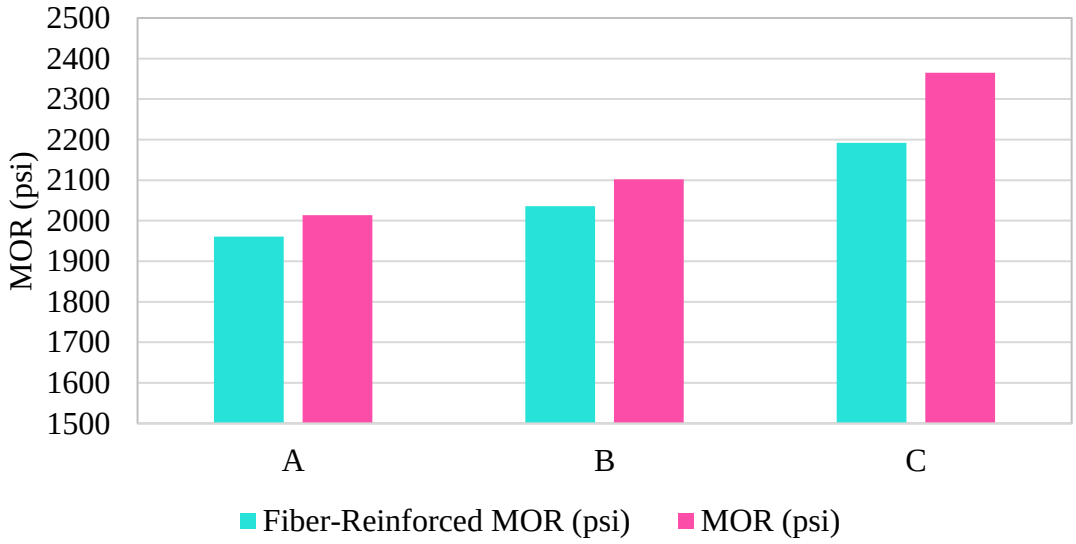

Figure 5.9 MOR of Unreinforced UHPC

Both the fiber-reinforced and unreinforced specimens exceeded the expected for specimens not heat cured compared to results in the literature (Aghdasi et al, 2016; Russel and Graybeal, 2013). The fiber-reinforced specimens of Mix A and Mix B have similar MOR values, around 2,000 psi, with Mix C performs slightly better around

2,200 psi. The general trend is repeated for the unreinforced specimens, though the first cracking strength occurred at loads 1%, 5%, and 14% greater than their reinforced counterparts, respectively.

The increase in the MOR of the unreinforced specimen may be a result of the different section properties, as UHPC has been shown to produce exaggerated size effects compared to typical concrete (Aghdasi et al., 2016). However, the difference could be related to the significantly different crack patterns of the reinforced and unreinforced specimens. Samples of the reinforced crack patterns are shown in Figure 5.10 and Figure 5.11.

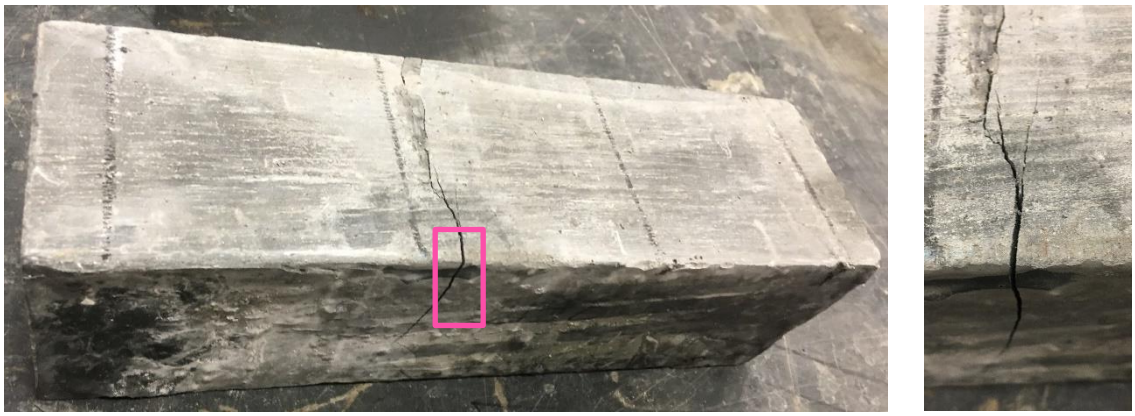

Figure 5.10 Crack Pattern of Fiber-Reinforced MOR Specimen

The images in Figure 5.10 show the reinforced specimens had cracked, but the crack was not wide enough to visibly show the fibers bridging. All three MOR specimens of Mix A had cracks that propagated through the bottom of the specimen through the top of the specimen, though none of those cracks were wider than that shown in Figure 5.10. The height of the crack upward, about 2/3 up the specimen shown in Figure 5.10, was typical for the specimens of Mix B and Mix C. This may suggest

that the mix with fly ash and VCAS™ did not bond with the fibers as well as the mixes with GGBFS.

Figure 5.11 Crack Pattern of Unreinforced MOR Specimens

The image in Figure 5.11 show the atypical cracking pattern of the unreinforced specimens. Each of the nine specimens tested shows a similar pattern of an arched crack. The crack begins vertically at the bottom surface where it begins to propagate. Gradually the entire cross-section of the specimen begins to curve, getting progressively steeper with no consistent direction, to an angle of nearly 45° an eighth of an inch from the top of the specimen, where the crack sharply cuts in the other direction. The "cut-back" point of the crack varies from a sixteenth inch to a quarter inch from the top surface of the specimen. The extended line of the crack indicates the concrete consumed more energy upon propagation than a typical straight-line crack.

Altogether, the MOR of the unreinforced and reinforced specimens exceeded the expectations based on previous research, with all exceeding 1.8 ksi, and Mixes B and Mixes C and exceeding 2.0 ksi. The MOR of the unreinforced specimens was

consistently higher than the fiber-reinforced specimens. This may be due in part to the size effect, or the additional energy dissipated during cracking.

5.5 Non-Compressive Testing Summary

In this study, the mixes tested had MOE values of approximately 5,500 ksi, and Mix B had a slightly lower MOE than Mix A and Mix C. While the ACI equation (Equation 5.1) overestimates this value, the model proposed by Russel and Graybeal (Equation 5.2) was extremely accurate, within 1% of actual MOE values.

The abrasion resistance of Ductal® was found to be superior to that of the non-proprietary mixes on the cast surface. However, Mixes A, B, and C had troweled surfaces with superior abrasion resistance to Ductal®, because the surfaces were smoother. Further study is required to compare ground-smooth surfaces of these mixes.

The MOR of unreinforced specimens was greater or higher than the MOR of the first crack of the reinforced specimens, likely due to a combination of the size effect and the increased fracture energy required to crack through the curved surface of the unreinforced specimens. Mixes A, B, and C increased in MOR in that order, with Mixes B and C exceeding a MOR strength of 2,000 psi. The MOR of all three developed mixes exceeded anticipated values based on a review of previous research studies.

6 Findings, Conclusions, and Recommendations

The following chapter summarizes the findings, conclusions, and recommendations from this research study.

6.1 Findings

The following findings were observed over the course of this study:

- Variations in material between sources makes reproducing published non-proprietary mixes untenable.
- The compressive strength of UHPC could vary up to 18% from no consolidation to high frequency consolidation for an extended period of time.
- HRWR did not influence the mortar flow of a mix as much as a varying w/cm ratio.
- W/cm ratios less than 0.2 were untenable, as the amount of HRWR needed to compensate for the lack of mortar flow made the mixture sticky and unworkable.
- Combinations of SCMs that vary by only 5% can produce mixes with dramatically different mortar flows and compressive strengths; similar mixes may not share similar properties.
- The chemical compatibility of constituents was more significant than the physical (particle packing) compatibility.
- A UHPC mix design cannot be determined with the exclusive application of the modified Andersen and Andreasen particle packing model.
- Particle packing defined by the modified Andersen and Andreasen model does not affect mortar flow or compressive strength.

- Mixes in this study that do not meet 5 in. of mortar flow do not "break," or slacken into flow.
- There is no combination of Type I and Type III cements in this study that provided a strength advantage at 28 days.
- There was no general correlation between aggregate/cementitious materials ratios and compressive strength, because the ideal aggregate/cementitious material ratio changed per different mixes.
- GGBFS mixes resulted in higher strength mixes when not combined with fly ash, and GGBFS mixes were stronger than fly ash mixes.
- Manufactured ground silica did not lead to strength increases compared to sand.
- The strongest mixes have 40-50% cumulative SCM replacement, with 10-12.5% silica fume.
- Fibers settled in mixes with mortar flows exceeding 8.25 in.
- Fibers did not increase the compressive strength of the concrete, but not prevent exploding failures.
- Heat curing for 36 hours at 180°F (82°C) produced 28-day compressive strengths at 3 days.
- A majority of the strength gain of heat curing occured in the first 12 hours for GGBFS mixes, and 36 hours for fly ash and VCAS™ mixes.
- Fiber-reinforced heat cured specimens outperformed unreinforced heat cured specimens.
- Formulated mixes have a MOE of approximately 5,500 ksi, which is accurately modeled by the Russel and Graybeal equation (2013).

- Ductal® had superior abrasion resistance compared to the formulated mixes on the cast surface.
- Formulated mixes have superior abrasion resistances compared to Ductal® on the troweled surface, due to their increased surface smoothness.
- Each of the formulated mixes had unreinforced MOR values exceeding 2,000 psi.
- The first-cracking MOR of reinforced specimens is less than the MOR of the unreinforced specimens.
- Curved surface crack patters of unreinforced flexure specimens absorbed more energy upon cracking than typical concrete specimens.

6.2 Conclusions

Based on the previously outlined findings, the following conclusions were developed:

- A proprietary mix design that met the FHWA definition of UHPC – 21.7 ksi compressive strength, 0.72 post-cracking tensile strength, and mortar flow exceeding 8 in. was not achieved in this study.
- Mix B (J3), with 2% by volume Grade 430 steel fibers and 36 hours of heat curing at 180°F (82°C), achieved a compressive strength of 20 ksi in 3 days.
- There lacked any evidence that the modified Andersen and Andreasen model was useful in developing a UHPC mix design, given that there was no correlation between the particle packing of the mix and the mortar flow or compressive strength.

- Heat curing the concrete is vital to achieving the high early strength that is one of UHPC's key advantages.
- The optimal mix design for materials readily available in the State of Oklahoma uses 10% silica fume, 30-40% GGBFS, Type I cement, a w/cm ratio of 0.2, an aggregate/cementitious material ratio of 1.0 when the aggregate is washed, fine sand, and sufficient HRWR reducer to produce a mortar flow of 7-8 in.

6.3 Recommendations

The goal of this study was to create a non-proprietary UHPC mix design using materials available in the State of Oklahoma, as well as developing an effective mixing, consolidation, and heat curing method. The findings and conclusions drawn from the research led to the following recommendations for future study:

- Investigate the effect of temperature of heat curing and the effect of applying heat curing earlier in the setting process.
- Investigate the effect of heat curing on the tensile and durability properties.
- Investigate long-term compressive strengths with and without heat curing.
- Investigate the necessity of grinding off the surface in-field.

References

Aghdasi, Parham, Heid, Ashley E., Chao, Shin-Ho, "Developing Ultra-High-Performance Fiber-Reinforced Concrete for Large-Scale Structural Applications," ACI Materials Journal, Vol. 133, No. 5, Sep.-Oct. 2016, pp. 559-570.

Alkaysi, Mouhammed, El-Tawil, Sherif, “Structural Response of Joints Made with Generic UHPC,” Structures Congress 2015, 2015, pp. 1435-1445.

Allena, Sriniva, Newston, Craig M., “Shrinkage of Fiber-Reinforced Ultrahigh Strength Concrete,” Journal of Materials in Civil Engineering, May 2012, pp. 612-615.

Alsalman, Ali, Canh, N. Dang, Hale, W. Micah, "Development of Ultra-high Performance Concrete with Locally Available Materials," Construction and Building Materials, Vol. 133, 2017, pp. 135-145.

American Concrete Institute, “Field Reference Manual: Specification for Structural Concrete ACI 301-05,” Publication SP-15 (05), pp. 489.

American Concrete Institute, “Cementitious Materials for Concrete,” ACI E3-13,” Aug. 2013, pp. 1-30.

Andersen, J., Andreasen, A.H.M., “About the Relationships Between Grain and Gradation Gap in Products of Loose Grains (With A Few Experiments),” Colloid Magazine, Vol. 50 Ed. 3, 1930, pp. 217-228 (in German).

Brouwers, H.J.H, Radix, H.J., “Self-Compacting Concrete: The Role of the Particle Size Distribution,” First International Symposium on Design, Performance, and Use of Self-Consolidation Concrete, 26-28 May 2005, pp. 109-118.

Fennis, Sonja, Walraven, Joost, “Using Particle Packing Technology for Sustainable Concrete Mixture Design,” HERON, Vol, 57 Ed. 2, 2012, pp. 73-102.

Funk, J.E., Dinger, D.R., “Predictive Process Control of Crowded Particulate Suspensions,” Applied to Ceramic Manufacturing, 1994.

Ghafari, Ehsan, Costa, Hugo, Julio, Eduardo, “Critical Review on Eco-Efficient Ultra-High Performance Concrete Enhanced with Nano-Materials,” Construction and Building Materials, Oct. 2015, pp. 201-208.

Graybeal, Ben, “Design and Construction of Field-Cast UHPC Connections,” FHWA-HRT-14-084, Oct. 2014, pp. 1-36.

Graybeal, Ben, “Development of Non-Proprietary Ultra-High Performance Concrete for Use in the Highway Bridge Sector,” FHWA-HRT-13-100, Oct. 2013, pp. 1-8.

Graybeal, Benjamin, Tanesi, Jussara, “Durability of an Ultrahigh-Performance Concrete,” Journal of Materials in Civil Engineering, Oct. 2007, pp. 848-854.

Graybeal, Ben, “Material Property Characterization of Ultra-High Performance Concrete,” FHWA-HRT-06-103, Aug. 2006, pp. 1-188.

Graybeal, Ben, “Ultra-High Performance Concrete,” FHWA-HRT-11-038, 2011, pp. 1-8.

Ibrahim, Ahmed, El-Chabib, Hassan, Eisa, Ahmed, “Ultrastrength Flowable Concrete Made with High Volumes of Supplementary Cementitious Materials,” Journal of Materials in Civil Engineering, Dec. 2013, pp. 1830-1839.

Kim, Heeae, Koh, Taehoon, Pyo, Sukhoon, “Enhancing Flowability and Sustainability of Ultra-High Performance Concrete Incorporating High Replacement Levels of Industrial Slags,” Construction and Building Materials, July 2016, pp. 153-160.

Randlinski, M., Harris, N.J., Moncarz, P.D., “Sustainable Concrete: Impacts of Existing and Emerging Materials and Technologies on the Construction Industry,” AEI 2011, 2011, pp. 252-262.

Russel, Henry G., Graybeal, Ben, “Ultra-High Performance Concrete: A State-of-the-Art Report for the Bridge Community,” FHWA-HRT-13-060, June 2013, pp. 1-176.

Sbia, Libya Ahmed, Peyvandi, Amirpasha, Lu, Jue, Abideen, Saqib, Weerasiti, Rankothge R., Balanchandra, Anagi M., Soroushian, Parviz, “Production Methods for Reliable Construction of Ultra-high-performance Concrete (UHPC) Structures," Materials and Structures, Vol. 50, No. 1, Aug. 2016, pp. 1-19.

“Supplementary Cementitious Materials: Best Practices for Concrete Pavements,” FHWA-HIF-16-001, Feb. 2016, pp. 1-7.

“VCAS™ White Pozzolans,” Vitro Minerals, www.vitrominerals.com

Van Dam, Thomas, “Supplementary Cementitious Materials and Blended Cements to Improve Sustainability of Concrete Pavements,” National Concrete Pavement Technology Center, Nov. 2013, pp. 1-8.

Yang, S.I., Millard, S.G., Soutsos, M. N., Barnett, S.J., Le, T.T., “Influence of Aggregate and Curing Regime on the Mechanical Properties of Ultra-High Performance Fiber Reinforced Concrete (UHPFRC),” Construction and Building Materials, Vol. 23, Mar. 2009, pp. 291-298.

Ye, Yinghua, Hu, Song, Daio, Bo, Yang, Songlin, Liu Zijian, "Mechanical Behavior of Ultra-High Performance Concrete Reinforced with Hybrid Different Shapes of Steel Fiber," CICTP (ASCE) 2012, 2012, pp. 3017-3028.

Yu, R., Spiesz, P., Brouwers, H.J.H., “Development of an Eco-Friendly Ultra-High Performance Concrete (UHPC) with Efficient Cement and Mineral Admixtures Uses,” Cement and Composites, Oct. 2015, pp. 383-394.

Appendix

The following tables display the mix designs proportions, mortar flows, and compressive strengths of the iterations series outlined in Chapter 3.

Table A.1 Series A Mix Design Proportions and Results

		A2	A3	A4	A5	A6	A7	A8	A9	A10
Type III Cement		0.7	0.7	0.75	0.7	0.7	0.7	0.7	0.7	0.7
Silica Fume		0.15	0.15	0.15	0.15	0.15	0.15	0.15	0.15	0.15
Fly Ash		0.15	0.15	0.1	0.15	0.15	0.15	0.15	0.15	0.15
w/cm		0.23	0.23	0.18	0.23	0.23	0.23	0.22	0.21	0.2
agg/cm		1.00	1.00	0.75	1.00	1.00	1.00	1.00	1.00	1.00
HRWR (oz./cwt)		21	22	22	18.7	21	16.3	18.7	18.7	18.7
Mortar Flow (in.)		10	10	6.781	10	10	9	9.583	8.625	6.917
Compressive Stength (psi)	1-Day	6040	6620	8900	7990	7320	6780	7590	7840	6970
	3-Day	9590	8110	11300	7780	8350	7470	9000	9690	9420
	7-Day	10010	9630	11450	9870	9820	9390	10170	11120	10500

Table A.2 Series A Mix Design Proportions and Results

		A11	A12	A13	A14	A15	A16	A17	A18	A19
Type III Cement		0.7	0.7	0.7	0.75	0.7	0.7	0.7	0.73	0.75
Silica Fume		0.15	0.15	0.15	0.2	0.2	0.15	0.15	0.14	0.13
Fly Ash		0.15	0.15	0.15	0.05	0.1	0.15	0.15	0.13	0.12
w/cm		0.23	0.23	0.23	0.23	0.23	0.23	0.23	0.23	0.23
agg/cm		0.90	0.80	0.70	1.00	1.00	1.00	1.00	1.00	1.00
HRWR (oz./cwt)		18.7	18.7	18.7	18.7	18.7	18.7	18.7	18.7	18.7
Mortar Flow (in.)		10	10	10	8.792	10	9.417	10.00	10.00	10.00
Compressive Stength (psi)	1-Day	7500	7770	7490	8430	8070	7600	8580	9280	8320
	3-Day	8860	8970	8890	8530	9290	6540	9800	10190	10580
	7-Day	9910	10560	10060	10740	10250	10290	10870	10570	11630

Table A.3 Series B Mix Design Proportions and Results

		B1	B2	B3	B4	B5	B6	B7	B8	B9
Type III Cement		0.75	0.75	0.75	0.75	0.75	0.75	0.75	0.75	0.75
Silica Fume		0.125	0.125	0.125	0.125	0.125	0.125	0.125	0.125	0.125
Fly Ash		0.125	0.125	0.125	0.125	0.125	0.125	0.125	0.125	0.125
w/cm		0.2	0.19	0.18	0.23	0.23	0.23	0.19	0.19	0.19
agg/cm		1.00	1.00	1.00	1.00	1.00	1.00	1.00	1.00	1.00
HRWR (oz./cwt)		18.7	18.7	18.7	16.3	14	11.67	21	23.33	25.66
Mortar Flow (in.)		8.0417	7.6667	6.458	9.75	8.625	7.158	7.542	6.7917	7.667
Compressive Stength (psi)	1-Day	9330	9970	9860	9140	9080	9460	10550	10550	10110
	3-Day	11140	11310	10850	10150	9680	10160	9810	10590	10600
	7-Day	11880	11080	11940	10260	10290	10960	11430	11780	11820

Table A.4 Series C Mix Design Proportions and Results

		C1	C2	C3	C4	C5	C6	C7	C8
Type III Cement		0.7	0.65	0.6	0.825	0.775	0.725	0.825	0.775
Silica Fume		0.125	0.125	0.125	0.05	0.1	0.15	0.125	0.125
VCAS ™		0	0	0	0	0	0	0	0
Fly Ash		0.125	0.125	0.125	0.125	0.125	0.125	0.05	0.1
GGBFS		0	0	0	0	0	0	0	0
Type I Cement		0.05	0.1	0.15	0	0	0	0	0
w/cm		0.201	0.201	0.201	0.201	0.201	0.201	0.201	0.201
agg/cm		1.00	1.00	1.00	1.00	1.00	1.00	1.00	1.00
HRWR (oz./cwt)		18.7	18.7	18.7	18.7	18.7	18.7	18.7	18.7
Mortar Flow (in.)			7.17	6.63	5.29	5.90	6.63	6.61	6.33
Compressive Stength (psi)	1-Day	12150	12160	11760	10650	10810	10120	11090	10400
	3-Day	10280	10430	10780	11550	11110	10840	11850	11570
	7-Day	10640	9040	9610	8130	9190	9040	11920	11510
	28-Day	14620						13110	12980

Table A.5 Series C Mix Design Proportions and Results

		C9	C10	C11	C12	C13	C14	C15	C16
Type III Cement		0.725	0.7	0.65	0.6	0.7	0.65	0.6	0.65
Silica Fume		0.125	0.125	0.125	0.125	0.125	0.125	0.125	0.05
VCAS ™		0	0	0	0	0.05	0.1	0.15	0
Fly Ash		0.15	0.125	0.125	0.125	0.125	0.125	0.125	0.1
GGBFS		0	0.05	0.1	0.15	0	0	0	0
Type I Cement		0	0	0	0	0	0	0	0.2
w/cm		0.201	0.201	0.201	0.201	0.201	0.201	0.201	0.2
agg/cm		1.00	1.00	1.00	1.00	1.00	1.00	1.00	1.00
HRWR (oz./cwt)		18.7	18.7	18.7	18.7	18.7	18.7	18.7	18.7
Mortar Flow (in.)		6.94	7.17	7.54	7.42	6.88	8.75	8.36	8.00
Compressive Stength (psi)	1-Day	9720	9400	9540	8820	9480	9600	9210	9490
	3-Day	10840	10800	10450	10170	8770	8980	8490	11300
	7-Day	11950	10790	11050	11570	11640	11520	10660	11820
	28-Day		12410	12660			13980	14900	13910

Table A.6 Series C Mix Design Proportions and Results

		C17	C18	C19	C20	C21	C22	C23	C24
Type III Cement		0.55	0.45	0.8	0.75	0.7	0.85	0.8	0.75
Silica Fume		0.05	0.05	0.1	0.15	0.2	0.05	0.05	0.05
VCAS ™		0	0	0	0	0	0	0	0
Fly Ash		0.1	0.1	0.1	0.1	0.1	0.1	0.15	0.2
GGBFS		0	0	0	0	0	0	0	0
Type I Cement		0.3	0.4	0	0	0	0	0	0
w/cm		0.2	0.2	0.2	0.2	0.2	0.2	0.2	0.2
agg/cm		1.00	1.00	1.00	1.00	1.00	1.00	1.00	1.00
HRWR (oz./cwt)		18.7	18.7	18.7	18.7	18.7	18.7	18.7	18.7
Mortar Flow (in.)		9.50	10.00	7.00	6.04	5.92	7.42	8.28	8.63
Compressive Stength (psi)	1-Day	10270	8580	9240	10190	9240	11610	10690	10760
	3-Day	11250	11260	10790	10690	10600	11360	10790	10530
	7-Day	12570	11690	12350	12620	11350	12310	11870	11610
	28-Day	14810	13810	13890	14550	13340	11930	13110	13880

Table A.7 Series D Mix Design Proportions and Results

		D1	D2	D3	D4	D5	D6	D7	D8
RSS		2.30916	2.314955	2.3092	2.6725	2.6662	2.6704	2.65397	2.647082
Type III Cement		0.15	0.1	0.05	0.1	0.1	0.05	0.05	0.05
Silica Fume		0.35	0.35	0.35	0.25	0.3	0.15	0.2	0.25
VCAS ™		0	0	0	0	0	0	0	0
Fly Ash		0.5	0.5	0.5	0.05	0	0.15	0.1	0.05
Type I Cement		0	0.05	0.1	0.6	0.6	0.65	0.65	0.65
w/cm		0.2	0.2	0.2	0.2	0.2	0.2	0.2	0.2
agg/cm		1.00	1.00	1.00	1.00	1.00	1.00	1.00	1.00
HRWR (oz./cwt)		18.7	18.7	18.7	18.7	18.7	18.7	18.7	18.7
Mortar Flow (in.)		4.75	4.75	4.833	5.5	4.942	7.042	6.108	6.8333
Compressive Stength (psi)	1-Day	0	0	0	6660	6650	6180	7470	6190
	3-Day	0	0	0	8710	9530	9200	9350	8350
	7-Day	4260	3580	3490	10210	10620	11360	10440	11070
	28-Day	5740	5470	5280	12630	12960	13060	13130	13060

Table A.8 Series D Mix Design Proportions and Results

		D9	D10	D11	D12	D13	D14	D15	D16	D17
RSS		2.65313	2.636141	2.6287						
Type III Cement		0	0	0	0.55	0.5	0.45	0.6	0.5	0.45
Silica Fume		0.1	0.15	0.2	0.125	0.125	0.125	0.05	0.05	0.125
VCAS ™		0	0	0	0.2	0.25	0.3	0	0	0
Fly Ash		0.2	0.15	0.1	0.125	0.125	0.125	0.1	0.1	0.125
Type I Cement		0.7	0.7	0.7	0	0	0	0.25	0.35	0.3
w/cm		0.2	0.2	0.2	0.2	0.2	0.2	0.2	0.2	0.2
agg/cm		1.00	1.00	1.00	1.00	1.00	1.00	1.00	1.00	1.00
HRWR (oz./cwt)		18.7	18.7	18.7	18.7	18.7	18.7	18.7	18.7	18.7
Mortar Flow (in.)		>10"	7.5	5.917	8.667	8.108	8.525	8.692	8.25	5.833
Compressive Stength (psi)	1-Day	6160	6540	6160	8280	7420	8650	9980	10790	9130
	3-Day	10670	8910	8650	9640	9370	8860	11490	11070	10980
	7-Day	11250	10100	7470	11680	10850	10750	12000	12300	11470
	28-Day	15840	12730	11760	13250	13500	14870	14130	13650	14100

Table A.9 Series E Mix Design Proportions and Results

		E1	E2	E3	E4	E5	E6	E7	E8
Type III Cement		0	0.1	0.15	0.2	0.25	0.3	0.35	0.4
Type I Cement		1	0.9	0.85	0.8	0.75	0.7	0.65	0.6
w/cm		0.2	0.2	0.2	0.2	0.2	0.2	0.2	0.2
cm/agg		1.00	1.00	1.00	1.00	1.00	1.00	1.00	1.00
agg/cm		18.70	18.70	18.70	18.70	18.70	18.70	18.70	18.70
Mortar Flow (in)		9.75	9.5	9	8.917	8.775	8.717	5.442	7.5833
Compressive Stength (psi)	1-Day	8440	8270	8750	8800	8820	8860	9250	9130
	7-Day	11040	9910	10070	10360	10250	10120	9930	10980
	28-Day	13200	11870	11540	11710	11860	11540	11860	11470

Table A.10 Series E Mix Design Proportions and Results

		E9	E10	E11	E12	E13	E14	E15
Type III Cement		0.45	0.5	0.6	0.7	0.8	0.9	1
Type I Cement		0.55	0.5	0.4	0.3	0.2	0.1	0
w/cm		0.2	0.2	0.2	0.2	0.2	0.2	0.2
cm/agg		1.00	1.00	1.00	1.00	1.00	1.00	1.00
agg/cm		18.70	18.70	18.70	18.70	18.70	18.70	18.70
Mortar Flow (in)		7.9167	7.1667	5.333	5.833	5.667	5.75	4.917
Compressive Stength (psi)	1-Day	9180	9800	9390	10600	10590	10770	10000
	7-Day	10170	10220	9840	11060	10650	10730	10040
	28-Day	11650	11490	11480	11440	11600	11930	10550

Table A.11 Series F Mix Design Proportions and Results

		F1	F2	F3	F4	F5	F6	F7	F8
		D9	C15	D14	C17	D9, 0.9 sand	C15, 0.9 sand	D14, .9 sand	C17, .9 sand
Type III Cement		0	0.6	0.45	0.55	0	0.6	0.45	0.55
Silica Fume		0.1	0.125	0.125	0.05	0.1	0.125	0.125	0.05
VCAS ™		0	0.15	0.3	0	0	0.15	0.3	0
Fly Ash		0.2	0.125	0.125	0.1	0.2	0.125	0.125	0.1
Type I Cement		0.7	0	0	0.3	0.7	0	0	0.3
w/cm		0.2	0.2009	0.201	0.201	0.2	0.201	0.201	0.2009
agg/cm		1.00	1.00	1.00	1.00	0.90	0.90	0.90	0.90
HRWR (oz./cwt)		18.7	18.7	18.7	18.7	18.7	18.7	18.7	18.7
Mortar Flow (in.)		8.67	5.92	7.08	10.50	9.75	7.00	8.08	10.00
Compressive Stength (psi)	**1-Day**	6190	8080	6580	9200	6040	8330	6760	10420
	7-Day	10910	10520	10320	11430	10290	10390	13160	10220
	28-Day	12170	11990	13070	12580	13540	12640	13090	13890

Table A.12 Series F Mix Design Proportions and Results

		F9	F10	F11	F12	F13	F14	F15	F16
		D9 .8 sand	C15, .8 sand	D14, .8 sand	C17, .8 sand	D9, 1.1 sand	C15 1.1 sand	D14, 1.1 sand	C17, 1.1 sand
Type III Cement		0	0.6	0.45	0.55	0	0.6	0.45	0.55
Silica Fume		0.1	0.125	0.125	0.05	0.1	0.125	0.125	0.05
VCAS ™		0	0.15	0.3	0	0	0.15	0.3	0
Fly Ash		0.2	0.125	0.125	0.1	0.2	0.125	0.125	0.1
Type I Cement		0.7	0	0	0.3	0.7	0	0	0.3
w/cm		0.2	0.2009	0.201	0.201	0.2	0.201	0.201	0.2009
agg/cm		0.80	0.80	0.80	0.80	1.10	1.10	1.10	1.10
HRWR (oz./cwt)		18.7	18.7	18.7	18.7	18.7	18.7	18.7	18.7
Mortar Flow (in.)		9.75	7.75	9.167	10	8	6	6.583	9
Compressive Stength (psi)	**1-Day**	6350	8470	7720	10310	7160	8950	7500	9670
	7-Day	11440	10940	10970	12200	10660	11030	10630	11490
	28-Day	13630	12790	13110	13280	13600	13510	14410	12430

Table A.13 Series G Mix Design Proportions and Results

		G1	G2	G3	G4	G5	G6	G7	G8	G9	G10
Type III Cement		0.85	0.75	0.65	0.55	0.8	0.7	0.6	0.5	0.75	0.65
Silica Fume		0.05	0.05	0.05	0.05	0.1	0.1	0.1	0.1	0.15	0.15
GGBFS		0.1	0.2	0.3	0.4	0.1	0.2	0.3	0.4	0.1	0.2
Type I Cement		0	0	0	0	0	0	0	0	0	0
w/cm		0.2	0.2	0.2	0.2	0.2	0.2	0.2	0.2	0.2	0.2
agg/cm		1.00	1.00	1.00	1.00	1.00	1.00	1.00	1.00	1.00	1.00
HRWR (oz./cwt)		18.7	18.7	18.7	18.7	18.7	18.7	18.7	18.7	18.7	18.7
Mortar Flow (in.)		6.75	8.125	9.75	10	5.525	6.833	7.5	9.75	5.917	6
Compressive Stength (psi)	**1-Day**	11660	10260	8930	8450	10160	10120	9350	7840	9380	9390
	7-Day	12360	12550	11250	12130	11990	11940	11030	11450	10500	11200
	28-Day	13830	13510	12830	13160	13090	10850	12980	12930	12960	12790

Table A.14 Series G Mix Design Proportions and Results

		G11	G12	G13	G14	G15	G16	G17	G18	G19	G20
Type III Cement		0.55	0.45	0.7	0.6	0.5	0.4	0.75	0.65	0.55	0.45
Silica Fume		0.15	0.15	0.2	0.2	0.2	0.2	0.05	0.05	0.05	0.05
GGBFS		0.3	0.4	0.1	0.2	0.3	0.4	0.1	0.1	0.1	0.1
Type I Cement		0	0	0	0	0	0	0.1	0.2	0.3	0.4
w/cm		0.2	0.2	0.2	0.2	0.2	0.2	0.2	0.2	0.2	0.2
agg/cm		1.00	1.00	1.00	1.00	1.00	1.00	1.00	1.00	1.00	1.00
HRWR (oz./cwt)		18.7	18.7	18.7	18.7	18.7	18.7	18.7	18.7	18.7	18.7
Mortar Flow (in.)		7.5	6.8333	5.042	5.608	5.3	6.383	6.667	7.5	7.417	8.5
Compressive Stength (psi)	1-Day	8230	6690	9600	9060	7780	6890	11110	11030	10770	9310
	7-Day	11550	10490	10150	10650	10300	10010	12840	13340	12460	12060
	28-Day	12420	13230	11480	12360	11870	12610	10620	14040	13660	13240

Table A.15 Series G Mix Design Proportions and Results

		G21	G22	G23	G24	G25	G27	G28	G29	G30	G31	G32
Type III Cement		0.65	0.55	0.45	0.35	0.5	0.3	0.2	0.4	0.3	0.2	0.1
Silica Fume		0.05	0.05	0.05	0.05	0.1	0.1	0.1	0.1	0.1	0.1	0.1
GGBFS		0.2	0.2	0.2	0.2	0.3	0.3	0.3	0.4	0.4	0.4	0.4
Type I Cement		0.1	0.2	0.3	0.4	0.1	0.3	0.4	0.1	0.2	0.3	0.4
w/cm		0.2	0.2	0.2	0.2	0.2	0.2	0.2	0.2	0.2	0.2	0.2
agg/cm		1.00	1.00	1.00	1.00	1.00	1.00	1.00	1.00	1.00	1.00	1.00
HRWR (oz./cwt)		18.7	18.7	18.7	18.7	18.7	18.7	18.7	18.7	18.7	18.7	18.7
Mortar Flow (in.)		8	9.1667	7.833	9.583	7.5	8.917	8.917	9.25	9.75	9.75	10.25
Compressive Stength (psi)	1-Day	8970	9180	8850	8690	8510	7920	6820	7510	6960	6340	5760
	7-Day	11190	10370	11030	11640	10860	11720	11010	11610	11820	11250	11620
	28-Day	12540	12190	12550	12770	12340	13620	12800	12970	13950	13370	13930

Table A.16 Series H Mix Design Proportions and Results

		H1	H2	H3	H4	H5	H6	H7	H8	H9
VCAS		0.00	0.00	0.00	0.00	0.00	0.00	0.00	0.00	0.00
Fly Ash		0.09	0.09	0.09	0.09	0.09	0.00	0.00	0.00	0.09
GGBFS		0.00	0.00	0.00	0.00	0.00	0.09	0.09	0.09	0.00
Type I Cement		0.81	0.81	0.81	0.81	0.81	0.81	0.81	0.81	0.81
agg/cm		1.16	1.42	1.42	1.42	1.42	1.42	1.42	1.42	1.42
Silica/ agg	10 Micrometers		0.11	0.18				0.11		
	15 Micrometers				0.11	0.18			0.11	
w/cm		0.20	0.20	0.20	0.20	0.20	0.20	0.20	0.20	0.20
HRWR (oz./cwt)		22.7	20.2	20.2	20.2	20.2	20.2	20.2	20.2	20.2
Mortar Flow (in.)		9.8333	9.75	9.75	7.25	7.667	7.042	8.1667	8	6.5
Compressive Stength (psi)	1-Day	7380	5840	6480	7440	6760	6970	6580	6300	6440
	7-Day	11610	10330	10860	8550	10430	10380	10630	10510	10250
	28-Day	14150	11570	12480	14300	12490	13330	13410	13150	12560

Table A.17 Series J Mix Design Proportions and Results

		J1	J2	J3	J4	J5	J6	J7
Type III Cement		0	0	0	0	0.55	0.55	0
Silica Fume		0.1	0.1	0.1	0.1	0.05	0.05	0.125
VCAS ™		0	0	0	0	0	0	0.15
Fly Ash		0	0	0	0	0.1	0.1	0.125
GGBFS		0.1	0.2	0.3	0.4	0	0	0
Type I Cement		0.8	0.7	0.6	0.5	0.3	0.3	0.6
w/cm		0.2	0.2	0.2	0.2	0.2	0.2	0.2
agg/cm		1.00	1.00	1.00	1.00	1.00	1.00	1.00
HRWR (oz./cwt)		18.7	18.7	18.7	18.7	23	23	18.7
Mortar Flow (in.)		8.69	9.75	10.25	15.00	6.08	9.00	9.50
Compressive Stength (psi)	1-Day	5840	7030	6010	5330	8870	9230	8850
	7-Day	11520	11810	12130	12140	10560	10740	11770
	28-Day	13270	13550	14840	14970	11400	11990	13920

Table A.18 Series J Mix Design Proportions and Results

		J8	J9	J10	J11	J12	J13
Type III Cement		0	0	0.3	0.1	0.3	0.1
Silica Fume		0.1	0.05	0.1	0.1	0.1	0.1
VCAS ™		0.15	0	0	0	0	0
Fly Ash		0.15	0.1	0	0	0	0
GGBFS		0	0	0.2	0.4	0.2	0.4
Type I Cement		0.6	0.85	0.4	0.4	0.4	0.4
w/cm		0.2	0.2	0.2	0.2	0.2	0.2
agg/cm		1.00	1.00	1.00	1.00	1.00	1.00
HRWR (oz./cwt)		18.7	18.7	18.7	18.7	18.7	18.7
Mortar Flow (in.)		13.00	6.00	9.00	7.50	5.17	10.00
Compressive Stength (psi)	1-Day	6080	8810	5750	6110	6740	8360
	7-Day	12520	12060	11050	11880	9830	10090
	28-Day	14030	13450	13470	14240	12260	14770